

InpaintDPO: Mitigating Spatial Relationship Hallucinations in Foreground-conditioned Inpainting via Diverse Preference Optimization

Qirui Li^{1*} Yizhe Tang^{1*} Ran Yi^{1†} Guangben Lu²
 Fangyuan Zou² Peng Shu² Huan Yu² Jie Jiang²
¹Shanghai Jiao Tong University ²Tencent

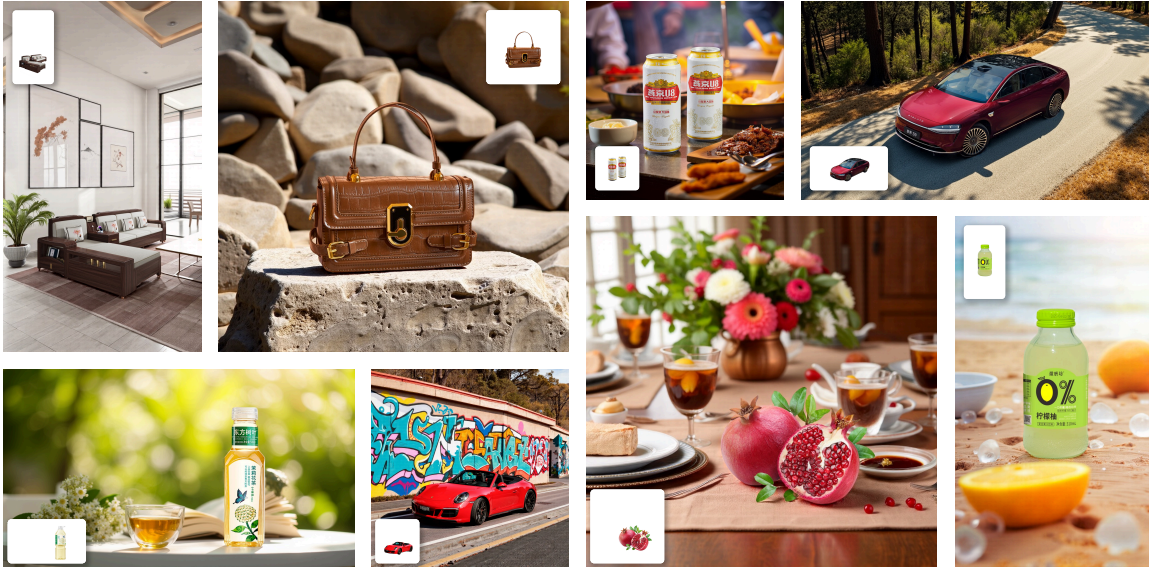


Figure 1. Our **InpaintDPO** generates high-quality images with plausible spatial relationships between foreground subject and background scene, while also achieving outstanding foreground consistency and text alignment.

Abstract

Foreground-conditioned inpainting, which aims at generating a harmonious background for a given foreground subject based on the text prompt, is an important subfield in controllable image generation. A common challenge in current methods, however, is the occurrence of Spatial Relationship Hallucinations between the foreground subject and the generated background, including inappropriate scale, positional relationships, and viewpoints. Critically, the subjective nature of spatial rationality makes it challenging to quantify, hindering the use of traditional reward-based RLHF methods. To address this issue, we propose **InpaintDPO**, the first Direct Preference Optimization (DPO) based framework dedicated to spatial rationality in foreground-conditioned inpainting, ensuring plausible spatial relationships between foreground and background elements. To resolve the gradient conflicts in standard DPO

caused by identical foreground in win-lose pairs, we propose **MaskDPO**, which confines preference optimization exclusively to the background to enhance background spatial relationships, while retaining the inpainting loss in the foreground region for robust foreground preservation. To enhance coherence at the foreground-background boundary, we propose **Conditional Asymmetric Preference Optimization**, which samples pairs with differentiated cropping operations and applies global preference optimization to promote contextual awareness and enhance boundary coherence. Finally, based on the observation that winning samples share a commonality in plausible spatial relationships, we propose **Shared Commonality Preference Optimization** to enhance the model’s understanding of spatial commonality across high-quality winning samples, further promoting shared spatial rationality. Extensive experiments demonstrate that **InpaintDPO** significantly mitigates Spatial Relationship Hallucinations, achieving superior performance in background spatial rationality while ensuring competitive foreground preservation and text-alignment. The code

*Equal contribution.

†Corresponding author. ranyi@sjtu.edu.cn

and models of our migration on Qwen-Image-Edit will soon be available at <https://github.com/Apple233/InpaintDPO>.

1. Introduction

Controllable image generation [6, 24, 25, 55, 66–68, 71] has seen remarkable progress, enabling the creation of highly realistic and diverse images. A crucial sub-field, foreground-conditioned background inpainting [9, 41, 56] stands out as a specialized task with direct applications in areas such as advertisement design and product promotion. It focuses on generating a text-aligned and contextually appropriate background for a given foreground object.

However, a prevalent issue in existing foreground-conditioned inpainting methods is the overemphasis on preserving the foreground features, which disrupts the model’s originally learned distribution, leading to “**Spatial Relationship Hallucinations**” where the generated background elements are positioned illogically relative to the foreground as in Fig. 2. These hallucinations can be classified into three categories: 1) Inappropriate Spatial Scale, where the foreground object often exhibits incorrect relative sizes compared to background references; 2) Inappropriate Positional Relationship, which is often observed as unsupported placement (objects appearing to float without physical support) or geometric errors (contact surface misalignment); 3) Inappropriate Viewpoint, where the camera viewpoint of the foreground mismatches that of the background scene.

Recently, with the successful application of RLHF in LLM [1, 10, 45], some T2I methods [5, 18, 58] have also attempted to use RLHF strategies to generate results that are more aligned with human preferences, especially based on a pretrained Reward Model [48, 63, 72] to improve overall aesthetic appeal or objective aspects, such as counting accuracy and prompt-image alignment. However, in our task, the core challenge is that the *spatial rationality* of an image is inherently subjective and difficult to quantify with any metric or pretrained model. This difficulty hinders the use of reward-based reinforcement learning strategies like PPO [5, 52] or GRPO [53, 64], which require a clear, computable reward signal. As a result, we turn to design a novel post-training methodology for spatial rationality enhancement based on Direct Preference Optimization (DPO) [49]. We first construct a customized human preference dataset by generating and filtering a large pool of background inpainting samples across diverse foreground subjects. Then we conduct rigorous manual annotation to establish a high-quality dataset of win-lose pairs based on the rationality of spatial relationships. By fine-tuning the model using our DPO-based approach, we aim to directly align the generation process with human preferences, yielding background synthesis that is spatially rational and visually harmonious.



Figure 2. Three categories of “**Spatial Relationship Hallucinations**” in foreground-conditioned inpainting, where previous methods [13, 33, 41] suffer from inappropriate spatial scale, spatial relationship and viewpoint. In contrast, our method can generate spatially rational images without such hallucinations.

While successful in some Text-to-Image (T2I) domains [36, 58, 65], directly applying standard DPO to enhance spatial rationality in foreground-conditioned inpainting faces a fundamental conflict. Since the task requires the foreground subject to be preserved as the given one, the foreground remains identical across winning and losing samples in a pair. Applying standard DPO, which optimizes the entire image, forces the model to simultaneously encourage and discourage the same foreground features. This conflicting signal results in model degradation such as missing details or incomplete denoising in the subject area.

To address this challenge, we propose **InpaintDPO**, a novel post-training method that establishes the first DPO-based framework dedicated to spatial rationality in foreground-conditioned inpainting, ensuring plausible spatial relationships between foreground and background elements.

Firstly, to resolve the gradient conflict in standard DPO caused by identical foregrounds across the win-lose pairs, we propose **MaskDPO**, which leverages the foreground mask to confine the DPO optimization to the background, applying preference learning only where needed. Simultaneously, to guarantee robust foreground subject preservation, we retain the original inpainting loss within the foreground subject area. This spatially disentangled optimization mechanism enables MaskDPO to refine background spatial relationships without compromising the preservation of the foreground subject. Secondly, to enhance coherence at the foreground-background boundary, we propose **Conditional Asymmetric Preference Optimization (CAPO)**, which performs global preference optimization to win-lose pairs that differ in foreground positioning, achieved through differentiated cropping. This positional difference naturally prevents gradient conflict seen in standard DPO, while the subsequent global preference optimization effectively enhances the visual coherence at the foreground boundary. Thirdly, we observe that winning samples share common spatial relationship characteristics. To capture this commonality, we propose **Shared Commonality Preference**

Optimization (SCPO). Its goal is to make the model’s implicit rewards for high-quality winning samples not just high, but also concentrated. By narrowing the implicit reward gap between win-win pairs, SCPO explicitly teaches the model to capture and enhance the shared spatial relationship characteristics that lead to success.

Extensive comparative experiments demonstrate that our InpaintDPO achieves significant gains in background spatial relationship rationality, while also maintaining superior performance in foreground consistency and text alignment.

We summarize our contributions as follows:

1. We propose InpaintDPO, the first DPO-based framework to address spatial relationship hallucination in foreground-conditioned inpainting, and a dedicated human preference dataset for spatial rationality alignment.
2. We propose MaskDPO to resolve standard DPO’s gradient conflict by confining preference optimization only to background region, enhancing background spatial relationships while preserving the foreground through inpainting loss.
3. We propose Conditional Asymmetric Preference Optimization to enhance coherence at the foreground boundary via conflict-free global preference optimization with differentiated cropping, effectively promoting contextual awareness and enhancing boundary coherence.
4. We propose Shared Commonality Preference Optimization, which captures the commonality of plausible spatial relationships by narrowing implicit reward gap among high-quality winning samples, further promoting shared spatial rationality.

2. Related Work

2.1. Image Inpainting

With remarkable advancements in Text-to-Image (T2I) diffusion model [17, 32, 46, 47, 51], a variety of diffusion-based inpainting methods have been proposed [3, 8, 16, 23, 28, 41, 42, 75]. Current methods can be broadly categorized into three groups: 1) Sampling-based methods [2, 3, 8, 12, 59] modify latent features during the diffusion process to incorporate given regions. But it often disrupts the original latent space distribution, leading to semantic inconsistencies or spatial artifacts. 2) Fine-tuning based methods [33, 42, 55, 69, 75] adapt the pre-trained T2I model structure for specific inpainting tasks. However, they are prone to catastrophic forgetting, which affects the pre-learned general knowledge, limiting the quality and diversity of generated images. 3) Condition-injecting methods [9, 13, 16, 19, 28, 56] inject features of given area into a frozen T2I backbone via an external branch. However, with the increasing scale of base models, the branch networks become larger, leading to parameter overhead and high computational costs. Some methods [41, 56, 70] turn to train

a light-weight adapter for effective condition injection. But due to the lack of spatial information perception, sometimes their results contain spatial relationship hallucinations. We base on the state-of-the-art foreground-conditioned inpainting model FLUX-Pinco [41] and perform a DPO-based post-training to achieve better spatial relationships.

2.2. RLHF for T2I model

Reinforcement Learning from Human Feedback (RLHF) is a paradigm designed to align model with complex human preferences [1, 10, 30], which mostly involves a Reward Model (RM) trained on human-annotated data and fine-tunes the generative model using the RM’s predicted score as a learning signal. With the widespread application of RLHF on LLM [45, 49, 52, 53], some reinforcement learning based methods designed for T2I diffusion models have emerged [5, 18, 58, 63, 65]. Current T2I RLHF methods can be categorized into two types based on their optimization strategy: 1) Reward-Model based methods [5, 18, 26, 39, 63, 64, 73] usually pretrained a separate reward model [31, 48, 61, 63, 72] based on human preference data or utilize Vision-Language Model to assign a scalar reward to generated images. The model is then fine-tuned using RL techniques like PPO [52] or GRPO [53] to maximize this predicted reward signal. While effective in aligning models to subjective human standards, this approach is limited by the accuracy and convergence of the reward model [11]. 2) DPO-based methods [27, 29, 35, 36, 58, 65] directly optimize the T2I model using human preference data by reframing the optimization as a maximum likelihood problem [49] over the preference pairs, avoiding the explicit training and sampling steps required by the separate RM and RL phase. This strategy is more computationally efficient and enables more stable training, but requires an extensive collection of high-quality comparative human preference data.

3. Inpaint DPO

Foreground-conditioned inpainting aims at generating a high-fidelity background conditioned on a text description, while preserving the integrity of the given foreground subject. A primary challenge in this task is to ensure spatial rationality between the foreground and generated background. Previous methods suffer from **Spatial Relationship Hallucinations**, generating illogical background elements manifesting as inappropriate scale, unsupported placement, and mismatched viewpoints. Therefore, we turn to DPO, a human preference alignment technique that directly optimizes on the preference likelihood without learning an explicit reward model. However, directly applying standard DPO to our task faces a critical issue, where the identical foreground across win-lose pairs exhibit conflicting optimization gradients, leading to model degradation over training. To address this issue, we propose **Inpaint-**

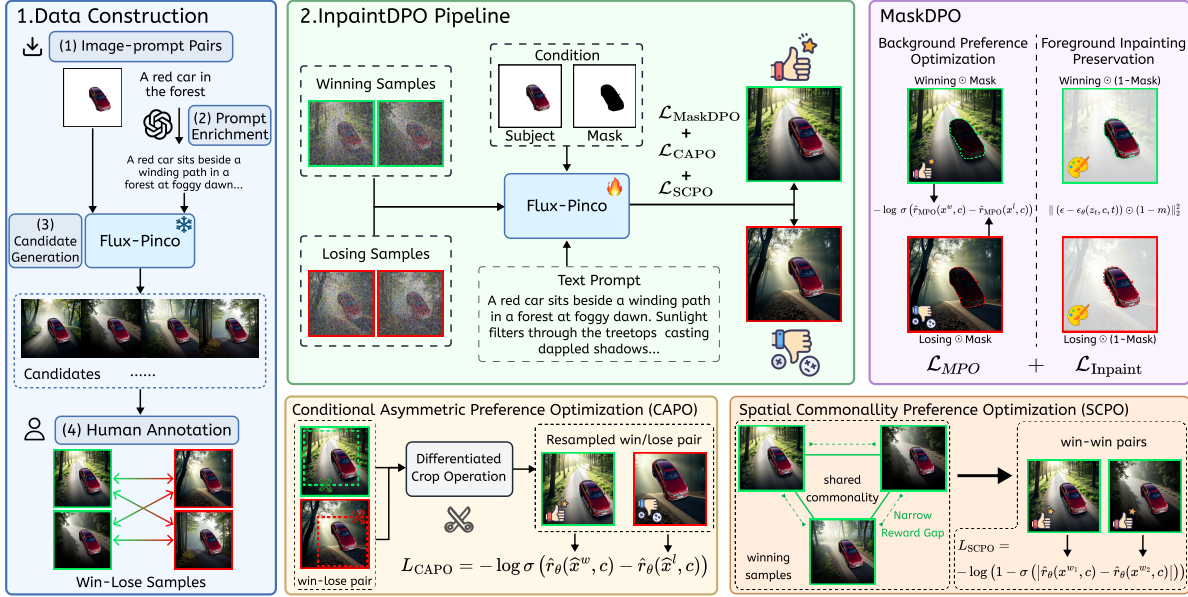


Figure 3. Overview of **InpaintDPO** framework for foreground-conditioned inpainting. 1) Data Construction: a four-stage pipeline to build the high-contrast spatial rationality human preference dataset. 2) InpaintDPO training pipeline and three proposed preference optimization strategies: MaskDPO confines preference optimization to background, while retaining inpainting loss for foreground preservation; CAPO enhances foreground boundary coherence through global preference optimization via differentiated cropping operation; SCPO captures the shared commonality of plausible spatial relationships of winning samples by narrowing implicit reward gap.

DPO, a novel DPO-based approach specifically designed to promote realistic and harmonious spatial relationships between the foreground and generated background. Crucially, InpaintDPO is a flexible preference optimization framework applicable to any existing diffusion-based foreground-conditioned inpainting model.

Specifically, to address the scarcity of foreground-conditioned win-lose pairs annotated for spatial relationship rationality, we first construct a large-scale high-quality foreground-conditioned inpainting dataset based on pre-trained model self-generation combined with high-standard manual annotation (Sec. 3.1). Then, to avoid the gradient conflict issue in standard DPO, we propose **MaskDPO**, a spatially disentangled optimization strategy that restricts the preference loss only in background region, while reusing the inpainting loss in the foreground region (Sec. 3.2). To enhance coherence at the foreground-background boundary, we propose **Conditional Asymmetric Preference Optimization**, which adjusts the position and size of foreground subject differently across win-lose pairs and performs a global preference optimization on entire images (Sec. 3.3). In addition, to fully capture the shared commonality of plausible spatial relationships in winning samples, we propose **Shared Commonality Preference Optimization**, which minimizes the reward gap between win-win pairs, to further promote spatial rationality (Sec. 3.4).

3.1. Spatial Rationality Preference Data

A fundamental obstacle to applying preference optimization techniques to foreground-conditioned inpainting is the

critical scarcity of specialized training datasets, as no public resource offers win-lose pairs specifically annotated for the **spatial rationality** between the foreground and background. Since the primary issue in this task is the occurrence of spatial relationship hallucinations, constructing a high-quality task-specific dataset that provides spatial rationality preference signals is a necessary prerequisite for training DPO-like strategies to yield visually consistent and human-preferred results.

To this end, we devised a four-stage data construction pipeline for spatial rationality human preference data. (1) First, we collected a large-scale set of subject image-prompt pairs from open-source repositories, which covers diverse common foreground subjects. (2) To increase the complexity and variation of the backgrounds, we employed GPT4o [1] for prompt expansion, generating richer descriptions of the background scene. (3) Then we utilized the state-of-the-art foreground-conditioned inpainting model FLUX-Pinco [32, 41] to generate a pool of 20 candidate background inpainted images for each case, ensuring a wide contrast range for preference labeling. (4) Finally, a rigorous human annotation and review process was implemented. Fifty professional annotators conducted a comprehensive evaluation based on text prompts, considering spatial rationality including spatial scale, positional relationship and viewpoint matching. Ultimately, 2-4 winning samples and 2-4 losing samples were selected for each case. This guarantees our dataset is specialized for our foreground-conditioned inpainting task, providing high-contrast spatial rationality win-lose preference signals re-

quired to optimize the model for superior spatial realism.

3.2. MaskDPO: Spatially Disentangled Optimization

Analysis of Standard DPO on Spatial Rationality Optimization. The standard DPO loss for Diffusion models [5] aims to maximize the log-probability gap between a winning sample x^w and a losing sample x^l . This is achieved by optimizing an implicit reward \hat{r}_θ derived from the policy model ϵ_θ and a reference model using ϵ_{ref} , formulated as:

$$L_{DPO} = \mathbb{E}_{(c, x^w, x^l) \sim D} \left[-\log \sigma \left(\hat{r}_\theta(x^w, c) - \hat{r}_\theta(x^l, c) \right) \right], \quad (1)$$

where the implicit reward \hat{r}_θ is typically a function of the L2-norm of the predicted noise error:

$$\hat{r}_\theta(x, c) \propto \mathbb{E}_{z_t, \epsilon} \left[\|\epsilon - \epsilon_{ref}(z_t, c, t)\|_2^2 - \|\epsilon - \epsilon_\theta(z_t, c, t)\|_2^2 \right]. \quad (2)$$

In foreground-conditioned inpainting, the condition c refers to the text prompt T and given foreground image, which are identical across the winning and losing samples in a human preference pair. The standard DPO loss (Eq. 1) calculates the preference optimization across the entire image, which aims to increase the probability of winning sample x^w and decrease the probability of losing sample x^l . However, since the foregrounds are identical in x^w and x^l in a training pair, this global loss forces the policy model ϵ_θ to learn completely **opposite gradient directions** within the foreground region. Specifically, the model is simultaneously pulled to increase and decrease the likelihood of generating the same foreground latent representation. Such conflicting gradients lead to model degradation and losing the ability to preserve foreground regions over training.

Masked Preference Optimization. To avoid the conflict, we propose Masked Preference Optimization (MPO), which performs spatially disentangled strategy constraining preference optimization only in the background region. We utilize the subject mask m (where $m = 1$ for the background) to reformulate the reward. Specifically, we first downsample and reshape the mask m to align it with the shape of z_t in diffusion. We compute the reward exclusively on the background region by multiplying this spatially-aligned mask m into the reward, effectively bypassing optimization on the identical foreground region that causes conflicting gradients. The reward \hat{r}_{MPO} is defined as:

$$\hat{r}_{MPO}(y, c) \propto \mathbb{E}_{z_t, \epsilon} \left[\|\epsilon - \epsilon_{ref}\|_2^2 \odot m - \|\epsilon - \epsilon_\theta\|_2^2 \odot m \right]. \quad (3)$$

This yields our preference loss L_{MPO} which applies DPO only to background area where distinct preferences exist:

$$L_{MPO} = \mathbb{E} \left[-\log \sigma \left(\hat{r}_{MPO}(x^w, c) - \hat{r}_{MPO}(x^l, c) \right) \right]. \quad (4)$$

Foreground Preservation Loss. While L_{MPO} successfully isolates the background for preference alignment, it provides no optimization signal to maintain the consistency of the foreground subject, in which case the model’s preservation of the foreground subject gradually decreases as

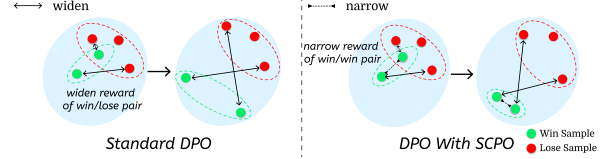


Figure 4. Comparison of Standard DPO and DPO with SCPO.

training progresses. To guarantee robust foreground preservation, we simultaneously apply the original inpainting loss, but constrain it only to the foreground region using $(1 - m)$:

$$L_{\text{Inpainting}} = \mathbb{E}_{x, t, \epsilon} \left[\|\epsilon - \epsilon_\theta(z_t, c, t)\|_2^2 \odot (1 - m) \right]. \quad (5)$$

Finally, our MaskDPO combines these two components:

$$L_{\text{MaskDPO}} = L_{MPO} + \lambda L_{\text{Inpainting}}, \quad (6)$$

where λ is a hyperparameter balancing background preference alignment and foreground preservation. This spatially disentangled optimization mechanism enables MaskDPO to refine background spatial relationships without compromising the preservation of the foreground subject.

3.3. Conditional Asymmetric Preference Optimization

While MaskDPO effectively improves rational spatial relationships within the background, its disentangled optimization does not explicitly address how the background interacts with foreground at boundary. Hence, we propose **Conditional Asymmetric Preference Optimization (CAPO)** to specialize in this interaction, ensuring a coherent and natural transition at the foreground-background boundary.

CAPO re-introduces a global preference optimization objective, but prevents gradient conflicts through a Differentiated Cropping Operation. By ensuring the positions of foreground subjects in winning and losing samples are not perfectly aligned pixel-by-pixel, our approach inherently prevents the gradient conflict observed in standard DPO, enabling stable full-image preference optimization with superior boundary coherence. Specifically, given a win-lose pair (x_0^w, x_0^l) , we apply different cropping operations to obtain \widehat{x}_0^w and \widehat{x}_0^l . This operation is designed to preserve subject integrity while deliberately assigning the subject to distinct relative spatial positions in the two images. Concurrently, we impose a Conditional Asymmetric Preference Optimization loss on the resulting \widehat{x}_0^w and \widehat{x}_0^l pairs:

$$L_{\text{CAPO}} = \mathbb{E}_{(c, \widehat{x}^w, \widehat{x}^l) \sim D} \left[-\log \sigma \left(\hat{r}_\theta(\widehat{x}^w, T) - \hat{r}_\theta(\widehat{x}^l, T) \right) \right]. \quad (7)$$

Such a Differentiated Cropping Operation can eliminate the gradient conflicts in standard DPO, while promoting the contextual awareness at the foreground boundary, thereby effectively enhancing boundary coherence.

3.4. Shared Commonality Preference Optimization

In our task, we observe that winning samples generated under the same conditions often share a significant **com-**

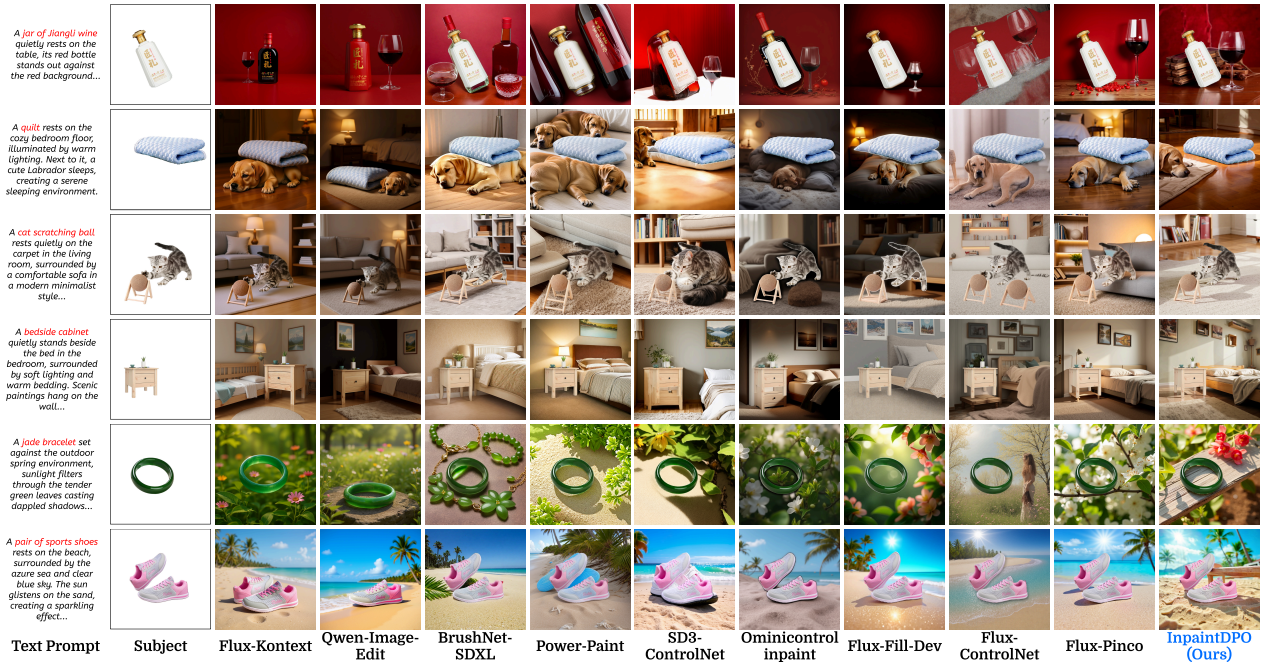


Figure 5. Qualitative comparison of existing inpainting or editing methods and our *InpaintDPO*. Our method generates plausible spatially rational images without hallucinations like inappropriate scale or position, with great prompt alignment and foreground consistency.

monality in their spatial layout and positional relationship. This suggests that favorable foreground-conditioned denoising trajectories in the latent space tend to exhibit a convergence around reasonable placements. Based on this observation, we propose **Shared Commonality Preference Optimization (SCPO)** to explicitly guide the model to capture this positional relationship commonality. SCPO encourages the model to narrow the implicit reward gap between win-win pairs, assigning high and close rewards for different winning samples, thereby reinforcing the shared and plausible spatial characteristics.

Different from DPO which aims to maximize the likelihood gap between winning samples x^w and losing samples x^l , the core idea of SCPO is to minimize the divergence of implicit rewards between two winning samples to assign similar values to both, as shown in Fig. 4. Specifically, SCPO is built upon the introduction of the win-win pair, consisting of two distinct human-preferred generated images (x^{w_1}, x^{w_2}) under the same condition c . We define the SCPO loss by measuring the absolute difference between the implicit rewards of a paired high-quality winning samples (c, x_1^w, x_2^w) $\in \mathcal{D}'$, where \mathcal{D}' is a dataset of win-win pairs. The loss is formulated using a symmetric, non-linear penalty function (detailed derivation in Suppl):

$$L_{\text{SCPO}} = \mathbb{E}_{(c, x^{w_1}, x^{w_2}) \sim \mathcal{D}'} [-\log(1 - \sigma(|\hat{r}_\theta(x^{w_1}, c) - \hat{r}_\theta(x^{w_2}, c)|))], \quad (8)$$

where the implicit reward \hat{r}_θ is the same as Eq. 2. By narrowing the gap of implicit rewards, the L_{SCPO} effectively promotes the model’s understanding of positional commonality within the win-win pair, leading to improved perceptual quality and structural consistency in generated results.

Also, it prevents the over-optimization of a singular winning sample and encourages a stable convergence of implicit reward over the winning data distribution.

Finally, our training loss is a weighted sum of the above three losses:

$$L = L_{\text{MaskDPO}} + \gamma L_{\text{CAPO}} + \mu L_{\text{SCPO}}, \quad (9)$$

where γ and μ are hyperparameters balancing the Loss terms L_{CAPO} and L_{SCPO} respectively.

4. Experiments

4.1. Experiment Settings

Dataset. The dataset for training our InpaintDPO was meticulously constructed, as detailed in Sec. 3.1. We began by collecting 3k high-quality image-prompt pairs from online inpainting data, reserving 500 pairs for evaluation. Subsequently, we generated masks using BiRefNet [74] and enriched the text prompts with GPT-4o [1]. Next, we generated 1k-resolution images across various aspect ratios (1:1, 9:16, and 16:9) using FLUX-Pinco [32, 41]. Finally, 50 professional annotators performed rigorous preference labeling, primarily focusing on spatial rationality. This process resulted in a comprehensive preference dataset containing over 10k win-lose pairs and 5k win-win pairs.

Implementation Details. We conduct our training on fine-tuning the FLUX-Pinco [32, 41] using LoRA [22, 57] (detailed architecture in Suppl). Our training is conducted on 8 NVIDIA 96G H20 GPUs for 5 epochs with a batch size of 2. During training, we adopt AdamW [40] optimizer and the learning rate was maintained at 0.0001, using a 1K-iteration

Table 1. Quantitative Comparisons with state-of-the-art inpainting methods. Best results are in red, second-best results are in blue.

Task	Methods	Metrics		Foreground Consistency		Spatial Rationality			Text-alignment		Image Quality	
		OER(BiRefNet) ↓	OER(SAM2.1) ↓	Scale ↑	Position ↑	Viewpoint ↑	VQAScore ↑	FV2Score ↓	FID ↓	Context ↑		
Edit	Flux-Kontext [34]	40.7%	44.0%	3.84	3.88	3.92	0.884	22.3%	111.43	0.159		
	Qwen-Image-Edit [60]	34.8%	23.7%	3.89	3.95	3.96	0.876	22.2%	115.72	0.254		
UNet-based Inpainting	PowerPaint [75]	27.4%	21.9%	3.44	3.61	3.84	0.744	12.7%	111.78	0.242		
	BrushNet [28]	18.3%	15.4%	3.57	3.71	3.46	0.826	9.4%	107.76	0.262		
MMDiT-based Inpainting	SD3-ControlNet [14]	22.3%	8.7%	3.72	3.68	3.78	0.873	12.6%	103.91	0.248		
	Ominicontrol-inpaint [55]	24.2%	8.4%	3.53	3.68	3.71	0.833	3.5%	117.29	0.254		
	Flux-Fill-dev [33]	12.3%	6.1%	3.74	3.48	3.56	0.820	9.0%	115.30	0.238		
	Flux-ControlNet [13]	16.7%	9.0%	3.63	3.72	3.80	0.870	3.3%	119.44	0.245		
	Flux-Pinco [41]	8.4%	4.3%	3.87	3.91	3.92	0.842	5.3%	99.05	0.249		
InpaintDPO	5.1%	2.7%	3.94	4.05	4.02	0.876	1.2%	96.43	0.268			

Table 2. User Study Results: ELO Ranking.

Rank	Method	ELO ↑	# Appearances	Rank	Method	ELO ↑	# Appearances
1	InpaintDPO	1432	2850	5	PowerPaint	871	2570
2	Pinco	1332	2570	6	Flux-Fill-dev	853	2180
3	BrushNet	1115	2310	7	OminiControl	784	2490
4	Flux-ControlNet	926	2110	8	SD3-ControlNet	686	2500

warmup. In Eq. 6 and 9, the hyperparameters λ , γ , μ are set to 2, 1 and 0.5 respectively.

Evaluation Metrics. Following Pinco [41], we comprehensively evaluate the performance of our model from four aspects: Image Quality, Foreground Consistency, Text-Alignment, and Spatial Rationality. (1) Image Quality: We utilize the Fréchet Inception Distance (FID) [20] on MSCOCO [37] to assess the overall realism and quality of the generated images. Also we follow OmniPaint [69] to evaluate the Context Coherence Score based on DINOv2 [44]. (2) Foreground consistency: To quantitatively measure the preservation and consistency of the foreground subject, we employ BiRefNet [74] and SAM2.1 [50] for accurate subject mask generation and then calculate the Object Extension Ratio (OER) [7] to evaluate the consistency between the subject shape in the generated image and the ground truth subject shape. (3) Text alignment: we use VQA Score [38] and FV2Score [62] to assess the subject-text alignment and the multi-subject rate. (4) Spatial rationality: we employ the multi-modal large language model GPT-4o [1] for an automated assessment of the subject’s positional rationality based on three aspects: spatial size, positional relationship, and viewpoint. Each aspect is scored on a scale of 1, 3, or 5.

4.2. Comparisons with Existing Methods

We conduct qualitative and quantitative comparisons, along with a user study, to demonstrate the superiority of our InpaintDPO. We compare with UNet-based inpainting methods, including PowerPaint [75] and BrushNet [28], and MMDiT-based inpainting methods including SD3-ControlNet [14], Flux-Fill-dev [33], Flux-ControlNet [13], Flux-OminiControl [55] and Flux-Pinco [41]. Additionally, we compare with two unified image generation and editing models, FLUX.1 Kontext [34] and Qwen Image [60], where we ask the model to perform background replacement while maintaining complete consistency of the input subject.

Qualitative Results. Fig. 5 shows the qualitative com-

Table 3. Quantitative Ablation Studies on Core Components: MaskDPO, CAPO, and SCPO.

Methods	Foreground Consistency		Spatial Rationality			Text-alignment		Image Quality			
	MaskDPO	CAPO	SCPO	OER(BiRefNet) ↓	OER(SAM2.1) ↓	Scale ↑	Position ↑	Viewpoint ↑	VQA Score ↑	FID ↓	Context ↑
✓				8.4%	4.3%	3.87	3.91	3.92	0.842	99.05	0.249
✓	✓			5.6%	3.4%	3.92	3.94	3.94	0.863	98.87	0.250
✓	✓	✓		5.6%	3.1%	3.90	3.96	3.92	0.866	97.42	0.258
✓	✓	✓	✓	5.1%	2.7%	3.94	4.05	4.02	0.876	96.43	0.268



Figure 6. Qualitative Ablation Studies on InpaintDPO’s Core Components.

parisons with previous inpainting and editing methods. In foreground-conditioned inpainting tasks, certain models face challenges in seamlessly integrating the subject with the background specified by prompts, as illustrated in the 2nd, 3rd, and 5th rows, leading to incorrect layout arrangements and object interaction. Furthermore, some methods struggle with subject expansion, a difficulty notably observed in the bedside table of the 4th row. For special subjects requiring multiple surfaces for support, as in 1st and 6th rows, several models find it problematic to accurately process this information, resulting in incorrect generation of just one single support surface. Notably, for editing methods, they possess fewer spatial relationship hallucinations, but suffer from a severe problem of foreground subject preservation, visibly deforming or changing the subjects required in inpainting task.

Quantitative Results. As presented in Table 1, our InpaintDPO achieves leading performance across various evaluation metrics. Regarding Image Quality, we achieve the best results, demonstrated by the lowest FID for high realism and the highest Context Coherence Score for superior contextual integration. For Foreground Consistency, our model outperforms in both OER scores, validating precise foreground preservation. Also, our model achieves the best spatial rationality in all three aspects, proving its enhanced ability to generate visually and spatially plausible

Table 4. Quantitative Ablation Studies on subject preservation in MaskDPO.

Combination	Foreground Consistency		Spatial Rationality			Text-alignment	Image Quality	
	OER(BiRefNet) ↓	OER(SAM2.1) ↓	Scale ↑	Position ↑	Viewpoint ↑	VQA Score ↑	FID ↓	Context ↑
Standard DPO	8.4%	4.3%	3.52	3.44	3.72	0.817	115.37	0.232
$L_{DPO} + L_{Subject-SCPO}$	7.8%	4.1%	3.93	3.92	3.94	0.858	99.37	0.246
$L_{MPO} + L_{Inpainting}$	5.6%	3.4%	3.92	3.94	3.94	0.863	98.87	0.250

Text Prompt Subject Pinco Standard DPO MPO+Subject-SCPO MPO+Inpaint loss (Ours)

Bad Spatial Rationality (floating) Bad Subject details Subject Expansion & color diff High Quality

Figure 7. Qualitative Ablation Comparisons of Pinco, standard DPO, MPO+Subject SCPO Loss and MaskDPO (Ours).

inpainting results. In terms of Text Alignment, Inpaint-DPO achieves lowest FV2Score and the highest VQAScore among inpainting models, being second only to editing models, which do trade off between subject preservation and image quality (as shown in Tab. 1 and Fig. 5, which is unacceptable for inpainting tasks).

User Study. We conducted a large-scale AI Inpainting Arena which employs the ELO rating system [15] to measure human preference to evaluate spatial rationality and perceptual quality (detailed setting in Suppl). We involve all the inpainting methods and invite 30 experts to choose images with better spatial rationality. After collecting over 10k votes, InpaintDPO achieved the highest ELO score, establishing a considerable lead over other models as in Tab. 2.

4.3. Ablation Study

Core Components. To investigate the effectiveness and individual contributions of the proposed modules MaskDPO, CAPO and SCPO, we conduct a comprehensive ablation study based on progressive additions, as detailed in Tab. 3 and Fig. 6. The introduction of MaskDPO yields the most significant improvement, particularly in improving spatial rationality (Fig. 6), and ensuring foreground consistency, reducing the OER(BiRefNet) substantially from 8.4% to 5.6%, validating the necessity of background preference alignment. Following this, integrating the CAPO further enhances the foreground boundary coherence, especially evidenced by improvements in Fig. 6 and perceptual metrics of Context score. The final inclusion of the SCPO introduces a further spatial rationality improvement, achieving the best overall performance across all quality metrics, proving the necessity and complementary nature of each module for advancing in foreground-conditioned inpainting.

Subject Preservation in MaskDPO. Our MaskDPO addresses the conflicting gradients in foreground region caused in Standard DPO by spatially disentangled optimization: background preference optimization and foreground inpainting loss. To validate its design, we compare MaskDPO with two alternative strategies: 1) Stan-

Table 5. Quantitative Comparisons for method migration on Qwen-Image-editing.

Method	Foreground Consistency		Spatial Rationality			Text-alignment	Image Quality	
	OER(BiRefNet) ↓	OER(SAM2.1) ↓	Scale ↑	Position ↑	Viewpoint ↑	VQA Score ↑	FID ↓	Context ↑
Qwen-Image-Edit	34.8%	23.7%	3.89	3.95	3.96	0.876	115.72	0.254
Qwen-Inpaint DPO	13.7%	9.4%	4.03	3.97	3.96	0.878	105.19	0.262

Text Prompt Subject Qwen-Image-Edit Qwen-InpaintDPO

Figure 8. Qualitative Comparisons between Qwen-Image-Edit and Qwen-InpaintDPO.

ard DPO, and 2) replacing the foreground inpainting loss $L_{Inpainting}$ with SCPO, minimizing the implicit reward within foreground for subject preservation. As shown in Fig. 7 and Tab. 4, Standard DPO can hardly preserve the subject. Replacing $L_{Inpainting}$ with foreground SCPO sometimes suffers from subject extension and color differences. In contrast, our MaskDPO effectively addresses these limitations, well preserves subject details and suppresses subject expansion, making it a more effective solution for subject preservation, which is crucial for high-quality inpainting tasks.

4.4. Method Migration

To validate the robustness and generalizability of our proposed InpaintDPO, we further conduct a transferability experiment by applying our InpaintDPO to an entirely different base model: the Qwen-Image-edit [60] (detailed settings in Suppl). Specifically, as shown in Tab. 5 and Fig. 8, applying InpaintDPO successfully enabled the image editing model to achieve better subject detail preservation and improved spatial rationality. It demonstrates that our InpaintDPO is a generic and effective strategy for mitigating the Spatial Relationship Hallucinations while preserving foreground subjects in foreground-conditioned inpainting task.

5. Conclusion

In this paper, we address the prevalent and challenging Spatial Relationship Hallucinations in foreground-conditioned inpainting, where existing models suffer from inappropriate spatial scale, positional relationship, and viewpoint between the given subject and generated background. Due to the subjectivity and poor quantifiability of spatial rationality, we propose InpaintDPO, a novel post-training framework dedicated to enhancing spatial rationality for this task via diverse preference optimization strategies. To resolve critical gradient conflicts of standard DPO in this scenario, we first introduce MaskDPO, which uses the foreground mask to confine preference optimization exclusively to the background while robustly preserving the foreground via inpainting loss. We further enhance foreground boundary

coherence through Conditional Asymmetric Preference Optimization, which employs differentiated cropping operation to boost contextual awareness. Finally, we propose Shared Commonality Preference Optimization to improve the model’s understanding of spatial commonalities across winning samples. Extensive experiments demonstrate that InpaintDPO significantly mitigates Spatial Relationship Hallucinations, achieving superior spatial rationality and visual quality compared to existing methods. Additionally, the successful transferability on Qwen-Image-edit validates its broad adaptability across different architectures.

References

- [1] Josh Achiam, Steven Adler, Sandhini Agarwal, Lama Ahmad, Ilge Akkaya, Florencia Leoni Aleman, Diogo Almeida, Janko Altenschmidt, Sam Altman, Shyamal Anadkat, et al. Gpt-4 technical report. *arXiv preprint arXiv:2303.08774*, 2023. 2, 3, 4, 6, 7, 14
- [2] Omri Avrahami, Dani Lischinski, and Ohad Fried. Blended diffusion for text-driven editing of natural images. In *Proceedings of the IEEE/CVF conference on computer vision and pattern recognition*, pages 18208–18218, 2022. 3
- [3] Omri Avrahami, Ohad Fried, and Dani Lischinski. Blended latent diffusion. *ACM transactions on graphics (TOG)*, 42(4):1–11, 2023. 3
- [4] Jason Baldridge, Jakob Bauer, Mukul Bhutani, Nicole Brich-tova, Andrew Bunner, Kelvin Chan, Yichang Chen, Sander Dieleman, Yuqing Du, Zach Eaton-Rosen, et al. Imagen 3. *arXiv preprint arXiv:2408.07009*, 2024. 15
- [5] Kevin Black, Michael Janner, Yilun Du, Ilya Kostrikov, and Sergey Levine. Training diffusion models with reinforcement learning. In *The Twelfth International Conference on Learning Representations*. 2, 3, 5
- [6] Jiazi Bu, Pengyang Ling, Yujie Zhou, Pan Zhang, Tong Wu, Xiaoyi Dong, Yuhang Zang, Yuhang Cao, Dahua Lin, and Jiaqi Wang. Hiflow: Training-free high-resolution image generation with flow-aligned guidance. *arXiv preprint arXiv:2504.06232*, 2025. 2
- [7] Binghui Chen, Chongyang Zhong, Wangmeng Xiang, Yifeng Geng, and Xuansong Xie. Virtualmodel: Generating object-id-retentive human-object interaction image by diffusion model for e-commerce marketing. *arXiv preprint arXiv:2405.09985*, 2024. 7, 14
- [8] Junsong Chen, Jincheng Yu, Chongjian Ge, Lewei Yao, Enze Xie, Yue Wu, Zhongdao Wang, James Kwok, Ping Luo, Huchuan Lu, et al. Pixart-alpha: Fast training of diffusion transformer for photorealistic text-to-image synthesis. *arXiv preprint arXiv:2310.00426*, 2023. 3
- [9] Xingye Chen, Wei Feng, Zhenbang Du, Weizhen Wang, Yanyin Chen, Haohan Wang, Linkai Liu, Yaoyu Li, Jinyuan Zhao, Yu Li, et al. Ctr-driven advertising image generation with multimodal large language models. In *Proceedings of the ACM on Web Conference 2025*, pages 2262–2275, 2025. 2, 3
- [10] Paul F Christiano, Jan Leike, Tom Brown, Miljan Martic, Shane Legg, and Dario Amodei. Deep reinforcement learn- ing from human preferences. *Advances in neural information processing systems*, 30, 2017. 2, 3
- [11] Kevin Clark, Paul Vicol, Kevin Swersky, and David J Fleet. Directly fine-tuning diffusion models on differentiable re- wards. In *The Twelfth International Conference on Learning Representations*, 2023. 3
- [12] Ciprian Corneanu, Raghudeep Gadde, and Aleix M Mar- tinez. Latentpaint: Image inpainting in latent space with diffusion models. In *Proceedings of the IEEE/CVF Winter Conference on Applications of Computer Vision*, pages 4334–4343, 2024. 3
- [13] AliMama Creative. Flux.1-dev controlnet inpainting beta. <https://huggingface.co/alimama-creative/FLUX.1-dev-Controlnet-Inpainting-Beta>, 2024. 2, 3, 7, 16
- [14] AliMama Creative. Sd3 controlnet inpainting. <https://huggingface.co/alimama-creative/SD3-Controlnet-Inpainting>, 2024. 7, 16
- [15] Arpad E Elo and Sam Sloan. The rating of chessplayers: Past and present. *Ishi Press*, 1978. 8, 16
- [16] Amir Erfan Eshratifar, Joao VB Soares, Kapil Thadani, Shaunak Mishra, Mikhail Kuznetsov, Yueh-Ning Ku, and Paloma De Juan. Salient object-aware background genera- tion using text-guided diffusion models. In *Proceedings of the IEEE/CVF Conference on Computer Vision and Pattern Recognition*, pages 7489–7499, 2024. 3
- [17] Patrick Esser, Sumith Kulal, Andreas Blattmann, Rahim Entezari, Jonas Müller, Harry Saini, Yam Levi, Dominik Lorenz, Axel Sauer, Frederic Boesel, et al. Scaling recti- fied flow transformers for high-resolution image synthesis. In *Forty-first International Conference on Machine Learn- ing*, 2024. 3
- [18] Ying Fan, Olivia Watkins, Yuqing Du, Hao Liu, Moonkyung Ryu, Craig Boutilier, Pieter Abbeel, Moham- mad Ghavamzadeh, Kangwook Lee, and Kimin Lee. Dpok: Reinforcement learning for fine-tuning text-to-image diffu- sion models. *Advances in Neural Information Processing Systems*, 36:79858–79885, 2023. 2, 3
- [19] Runze He, Kai Ma, Linjiang Huang, Shaofei Huang, Jialin Gao, Xiaoming Wei, Jiao Dai, Jizhong Han, and Si Liu. Freeedit: Mask-free reference-based image editing with multi-modal instruction. *arXiv preprint arXiv:2409.18071*, 2024. 3
- [20] Martin Heusel, Hubert Ramsauer, Thomas Unterthiner, Bernhard Nessler, and Sepp Hochreiter. Gans trained by a two time-scale update rule converge to a local nash equilib- rium. *Advances in neural information processing systems*, 30, 2017. 7, 16
- [21] Jonathan Ho, Ajay Jain, and Pieter Abbeel. Denoising dif- fusion probabilistic models. *Advances in neural information processing systems*, 33:6840–6851, 2020. 13
- [22] Edward J Hu, Yelong Shen, Phillip Wallis, Zeyuan Allen- Zhu, Yuanzhi Li, Shean Wang, Lu Wang, Weizhu Chen, et al. Lora: Low-rank adaptation of large language models. *ICLR*, 1(2):3, 2022. 6
- [23] Teng Hu, Jiangning Zhang, Ran Yi, Yuzhen Du, Xu Chen, Liang Liu, Yabiao Wang, and Chengjie Wang. Anomalyd- iffusion: Few-shot anomaly image generation with diffusion

- model. In *Proceedings of the AAAI conference on artificial intelligence*, pages 8526–8534, 2024. 3
- [24] Teng Hu, Jiangning Zhang, Ran Yi, Hongrui Huang, Yabiao Wang, and Lizhuang Ma. High-efficient diffusion model fine-tuning with progressive sparse low-rank adaptation. In *13th International Conference on Learning Representations, ICLR 2025*, pages 92066–92078. International Conference on Learning Representations, ICLR, 2025. 2
- [25] Teng Hu, Jiangning Zhang, Ran Yi, Jieyu Weng, Yabiao Wang, Xianfang Zeng, Zhucun Xue, and Lizhuang Ma. Improving autoregressive visual generation with cluster-oriented token prediction. In *Proceedings of the Computer Vision and Pattern Recognition Conference*, pages 9351–9360, 2025. 2
- [26] Zijing Hu, Fengda Zhang, Long Chen, Kun Kuang, Jiahui Li, Kaifeng Gao, Jun Xiao, Xin Wang, and Wenwu Zhu. Towards better alignment: Training diffusion models with reinforcement learning against sparse rewards. In *Proceedings of the Computer Vision and Pattern Recognition Conference*, pages 23604–23614, 2025. 3
- [27] Qihan Huang, Long Chan, Jinlong Liu, Wanggui He, Hao Jiang, Mingli Song, and Jie Song. Patchdpo: Patch-level dpo for finetuning-free personalized image generation. In *Proceedings of the Computer Vision and Pattern Recognition Conference*, pages 18369–18378, 2025. 3
- [28] Xuan Ju, Xian Liu, Xintao Wang, Yuxuan Bian, Ying Shan, and Qiang Xu. Brushnet: A plug-and-play image inpainting model with decomposed dual-branch diffusion. *arXiv preprint arXiv:2403.06976*, 2024. 3, 7, 16
- [29] Shyamgopal Karthik, Huseyin Coskun, Zeynep Akata, Sergey Tulyakov, Jian Ren, and Anil Kag. Scalable ranked preference optimization for text-to-image generation. In *Proceedings of the IEEE/CVF International Conference on Computer Vision*, pages 18399–18410, 2025. 3
- [30] Timo Kaufmann, Paul Weng, Viktor Bengs, and Eyke Hüllermeier. A survey of reinforcement learning from human feedback. 2024. 3
- [31] Yuval Kirstain, Adam Polyak, Uriel Singer, Shahbuland Matiana, Joe Penna, and Omer Levy. Pick-a-pic: An open dataset of user preferences for text-to-image generation. *Advances in neural information processing systems*, 36:36652–36663, 2023. 3
- [32] Black Forest Labs. Flux. <https://github.com/black-forest-labs/flux>, 2024. 3, 4, 6
- [33] Black Forest Labs. Flux-fill-dev. <https://github.com/black-forest-labs/flux/blob/main/docs/fill.md>, 2024. 2, 3, 7, 16
- [34] Black Forest Labs, Stephen Batifol, Andreas Blattmann, Frederic Boesel, Saksham Consul, Cyril Diagne, Tim Dockhorn, Jack English, Zion English, Patrick Esser, et al. Flux. 1 kontext: Flow matching for in-context image generation and editing in latent space. *arXiv preprint arXiv:2506.15742*, 2025. 7, 16
- [35] Shufan Li, Konstantinos Kallidromitis, Akash Gokul, Yusuke Kato, and Kazuki Kozuka. Aligning diffusion models by optimizing human utility. *Advances in Neural Information Processing Systems*, 37:24897–24925, 2024. 3
- [36] Zhanhao Liang, Yuhui Yuan, Shuyang Gu, Bohan Chen, Tiankai Hang, Mingxi Cheng, Ji Li, and Liang Zheng. Aesthetic post-training diffusion models from generic preferences with step-by-step preference optimization. In *Proceedings of the Computer Vision and Pattern Recognition Conference*, pages 13199–13208, 2025. 2, 3
- [37] Tsung-Yi Lin, Michael Maire, Serge Belongie, James Hays, Pietro Perona, Deva Ramanan, Piotr Dollár, and C Lawrence Zitnick. Microsoft coco: Common objects in context. In *Computer vision—ECCV 2014: 13th European conference, zurich, Switzerland, September 6–12, 2014, proceedings, part v 13*, pages 740–755. Springer, 2014. 7, 16
- [38] Zhiqiu Lin, Deepak Pathak, Baiqi Li, Jiayao Li, Xide Xia, Graham Neubig, Pengchuan Zhang, and Deva Ramanan. Evaluating text-to-visual generation with image-to-text generation. In *European Conference on Computer Vision*, pages 366–384. Springer, 2025. 7, 15
- [39] Jie Liu, Gongye Liu, Jiajun Liang, Yangguang Li, Jiaheng Liu, Xintao Wang, Pengfei Wan, Di Zhang, and Wanli Ouyang. Flow-grpo: Training flow matching models via online rl. *arXiv preprint arXiv:2505.05470*, 2025. 3
- [40] Ilya Loshchilov and Frank Hutter. Decoupled weight decay regularization. *arXiv preprint arXiv:1711.05101*, 2017. 6
- [41] Guangben Lu, Yuzhen Du, Yizhe Tang, Zhimin Sun, Ran Yi, Yifan Qi, Tianyi Wang, Lizhuang Ma, and Fangyuan Zou. Pinco: Position-induced consistent adapter for diffusion transformer in foreground-conditioned inpainting. In *Proceedings of the IEEE/CVF International Conference on Computer Vision*, pages 15266–15276, 2025. 2, 3, 4, 6, 7, 13, 16
- [42] Hayk Manukyan, Andranik Sargsyan, Barsegh Atanyan, Zhangyang Wang, Shant Navasardyan, and Humphrey Shi. Hd-painter: high-resolution and prompt-faithful text-guided image inpainting with diffusion models. *arXiv preprint arXiv:2312.14091*, 2023. 3
- [43] ModelScope. Diffsynth-studio. <https://github.com/modelscope/DiffSynth-Studio>, 2025. 17
- [44] Maxime Oquab, Timothée Darcet, Théo Moutakanni, Huy Vo, Marc Szafraniec, Vasil Khalidov, Pierre Fernandez, Daniel Haziza, Francisco Massa, Alaaeldin El-Nouby, et al. Dinov2: Learning robust visual features without supervision. *arXiv preprint arXiv:2304.07193*, 2023. 7, 16
- [45] Long Ouyang, Jeffrey Wu, Xu Jiang, Diogo Almeida, Carroll Wainwright, Pamela Mishkin, Chong Zhang, Sandhini Agarwal, Katarina Slama, Alex Ray, et al. Training language models to follow instructions with human feedback. *Advances in neural information processing systems*, 35:27730–27744, 2022. 2, 3
- [46] William Peebles and Saining Xie. Scalable diffusion models with transformers. In *Proceedings of the IEEE/CVF International Conference on Computer Vision*, pages 4195–4205, 2023. 3
- [47] Dustin Podell, Zion English, Kyle Lacey, Andreas Blattmann, Tim Dockhorn, Jonas Müller, Joe Penna, and Robin Rombach. Sdxl: Improving latent diffusion models for high-resolution image synthesis. *arXiv preprint arXiv:2307.01952*, 2023. 3

- [48] Alec Radford, Jong Wook Kim, Chris Hallacy, Aditya Ramesh, Gabriel Goh, Sandhini Agarwal, Girish Sastry, Amanda Askell, Pamela Mishkin, Jack Clark, et al. Learning transferable visual models from natural language supervision. In *International conference on machine learning*, pages 8748–8763. PmLR, 2021. 2, 3
- [49] Rafael Rafailov, Archit Sharma, Eric Mitchell, Christopher D Manning, Stefano Ermon, and Chelsea Finn. Direct preference optimization: Your language model is secretly a reward model. *Advances in neural information processing systems*, 36:53728–53741, 2023. 2, 3, 13
- [50] Nikhila Ravi, Valentin Gabeur, Yuan-Ting Hu, Ronghang Hu, Chaitanya Ryali, Tengyu Ma, Haitham Khedr, Roman Rädle, Chloe Rolland, Laura Gustafson, Eric Mintun, Junting Pan, Kalyan Vasudev Alwala, Nicolas Carion, Chao-Yuan Wu, Ross Girshick, Piotr Dollár, and Christoph Feichtenhofer. Sam 2: Segment anything in images and videos. *arXiv preprint arXiv:2408.00714*, 2024. 7, 14
- [51] Robin Rombach, Andreas Blattmann, Dominik Lorenz, Patrick Esser, and Björn Ommer. High-resolution image synthesis with latent diffusion models. In *Proceedings of the IEEE/CVF conference on computer vision and pattern recognition*, pages 10684–10695, 2022. 3
- [52] John Schulman, Filip Wolski, Prafulla Dhariwal, Alec Radford, and Oleg Klimov. Proximal policy optimization algorithms. *arXiv preprint arXiv:1707.06347*, 2017. 2, 3
- [53] Zhihong Shao, Peiyi Wang, Qihao Zhu, Runxin Xu, Junxiao Song, Xiao Bi, Haowei Zhang, Mingchuan Zhang, YK Li, Yang Wu, et al. Deepseekmath: Pushing the limits of mathematical reasoning in open language models. *arXiv preprint arXiv:2402.03300*, 2024. 2, 3
- [54] Jascha Sohl-Dickstein, Eric Weiss, Niru Maheswaranathan, and Surya Ganguli. Deep unsupervised learning using nonequilibrium thermodynamics. In *International conference on machine learning*, pages 2256–2265. pmlr, 2015. 13
- [55] Zhenxiong Tan, Songhua Liu, Xingyi Yang, Qiaochu Xue, and Xinchao Wang. Ominicontrol: Minimal and universal control for diffusion transformer. In *Proceedings of the IEEE/CVF International Conference on Computer Vision*, pages 14940–14950, 2025. 2, 3, 7, 16
- [56] Yizhe Tang, Zhimin Sun, Yuzhen Du, Ran Yi, Guangben Lu, Teng Hu, Luying Li, Lizhuang Ma, and Fangyuan Zou. Ata: Adaptive transformation agent for text-guided subject-position variable background inpainting. In *Proceedings of the Computer Vision and Pattern Recognition Conference*, pages 18335–18345, 2025. 2, 3
- [57] Chunlin Tian, Zhan Shi, Zhijiang Guo, Li Li, and Chengzhong Xu. Hydralora: An asymmetric lora architecture for efficient fine-tuning. *Advances in Neural Information Processing Systems*, 37:9565–9584, 2024. 6, 13
- [58] Bram Wallace, Meihua Dang, Rafael Rafailov, Linqi Zhou, Aaron Lou, Senthil Purushwalkam, Stefano Ermon, Caiming Xiong, Shafiq Joty, and Nikhil Naik. Diffusion model alignment using direct preference optimization. In *Proceedings of the IEEE/CVF Conference on Computer Vision and Pattern Recognition*, pages 8228–8238, 2024. 2, 3
- [59] Yikai Wang, Chenjie Cao, Junqiu Yu, Ke Fan, Xiangyang Xue, and Yanwei Fu. Towards enhanced image inpainting: Mitigating unwanted object insertion and preserving color consistency. In *Proceedings of the Computer Vision and Pattern Recognition Conference*, pages 23237–23248, 2025. 3
- [60] Chenfei Wu, Jiahao Li, Jingren Zhou, Junyang Lin, Kaiyuan Gao, Kun Yan, Sheng-ming Yin, Shuai Bai, Xiao Xu, Yilei Chen, et al. Qwen-image technical report. *arXiv preprint arXiv:2508.02324*, 2025. 7, 8, 16
- [61] Xiaoshi Wu, Yiming Hao, Keqiang Sun, Yixiong Chen, Feng Zhu, Rui Zhao, and Hongsheng Li. Human preference score v2: A solid benchmark for evaluating human preferences of text-to-image synthesis. *arXiv preprint arXiv:2306.09341*, 2023. 3
- [62] Bin Xiao, Haiping Wu, Weijian Xu, Xiyang Dai, Houdong Hu, Yumao Lu, Michael Zeng, Ce Liu, and Lu Yuan. Florence-2: Advancing a unified representation for a variety of vision tasks. In *Proceedings of the IEEE/CVF Conference on Computer Vision and Pattern Recognition*, pages 4818–4829, 2024. 7, 16
- [63] Jiazheng Xu, Xiao Liu, Yuchen Wu, Yuxuan Tong, Qinkai Li, Ming Ding, Jie Tang, and Yuxiao Dong. Imagereward: Learning and evaluating human preferences for text-to-image generation. *Advances in Neural Information Processing Systems*, 36:15903–15935, 2023. 2, 3
- [64] Zeyue Xue, Jie Wu, Yu Gao, Fangyuan Kong, Lingting Zhu, Mengzhao Chen, Zhiheng Liu, Wei Liu, Qiushan Guo, Weilin Huang, et al. Dancegrpo: Unleashing grpo on visual generation. *arXiv preprint arXiv:2505.07818*, 2025. 2, 3
- [65] Kai Yang, Jian Tao, Jiafei Lyu, Chunjiang Ge, Jiabin Chen, Weihai Shen, Xiaolong Zhu, and Xiu Li. Using human feedback to fine-tune diffusion models without any reward model. In *Proceedings of the IEEE/CVF Conference on Computer Vision and Pattern Recognition*, pages 8941–8951, 2024. 2, 3
- [66] Hu Ye, Jun Zhang, Sibio Liu, Xiao Han, and Wei Yang. Ip-adapt: Text compatible image prompt adapter for text-to-image diffusion models. *arXiv preprint arXiv:2308.06721*, 2023. 2
- [67] Ran Yi, Teng Hu, Mengfei Xia, Yizhe Tang, and Yong-Jin Liu. Feditnet++: Few-shot editing of latent semantics in gan spaces with correlated attribute disentanglement. *IEEE Transactions on Pattern Analysis and Machine Intelligence*, 2024.
- [68] Ran Yi, Teng Hu, Zihan Su, and Lizhuang Ma. Iar2: Improving autoregressive visual generation with semantic-detail associated token prediction. *arXiv preprint arXiv:2510.06928*, 2025. 2
- [69] Yongsheng Yu, Ziyun Zeng, Haitian Zheng, and Jiebo Luo. Omnipaint: Mastering object-oriented editing via disentangled insertion-removal inpainting. In *Proceedings of the IEEE/CVF International Conference on Computer Vision*, 2025. 3, 7, 16
- [70] Jianhui Zhang, Shen Cheng, Qirui Sun, Jia Liu, Wang Luyang, Chaoyu Feng, Chen Fang, Lei Lei, Jue Wang, and Shuaicheng Liu. Ultra high-resolution image inpainting with patch-based content consistency adapter. In *Proceedings of the IEEE/CVF International Conference on Computer Vision*, pages 16991–17000, 2025. 3

- [71] Lvmin Zhang, Anyi Rao, and Maneesh Agrawala. Adding conditional control to text-to-image diffusion models. In *Proceedings of the IEEE/CVF International Conference on Computer Vision*, pages 3836–3847, 2023. [2](#)
- [72] Tianyi Zhang, Varsha Kishore, Felix Wu, Kilian Q Weinberger, and Yoav Artzi. Bertscore: Evaluating text generation with bert. In *International Conference on Learning Representations*, . [2](#), [3](#)
- [73] Xinchun Zhang, Ling Yang, Guohao Li, YaQi Cai, Yong Tang, Yujiu Yang, Mengdi Wang, Bin CUI, et al. Itercomp: Iterative composition-aware feedback learning from model gallery for text-to-image generation. In *The Thirteenth International Conference on Learning Representations*, . [3](#)
- [74] Peng Zheng, Dehong Gao, Deng-Ping Fan, Li Liu, Jorma Laaksonen, Wanli Ouyang, and Nicu Sebe. Bilateral reference for high-resolution dichotomous image segmentation. *arXiv preprint arXiv:2401.03407*, 2024. [6](#), [7](#), [14](#)
- [75] Junhao Zhuang, Yanhong Zeng, Wenran Liu, Chun Yuan, and Kai Chen. A task is worth one word: Learning with task prompts for high-quality versatile image inpainting. *arXiv preprint arXiv:2312.03594*, 2023. [3](#), [7](#), [16](#)

Appendix

A. Overview

In this supplementary material, we mainly present the following contents:

- More implementation details of our model structure (Sec. B).
- Detailed derivation analysis of Shared Commonality Preference Optimization (Sec. C).
- More technical details of the evaluation metrics (Sec. D).
- More details of the user study (Sec. E).
- More qualitative comparisons with state-of-the-art inpainting and editing methods (Sec. F).
- More ablation study on the Conditional Asymmetric Preference Optimization (Sec. G).
- More experiments settings and results of method migration on Qwen-Image-Edit (Sec. H).
- More results of InpaintDPO with different aspect ratios (Sec. I).

B. Implementation Details

Backbone. We apply our proposed InpaintDPO on Flux-Pinco [41]. We use the VAE Encoder of the original Flux model as our semantic feature extractor and only take the output of the final layer as our semantic feature. Meanwhile, we also construct a simple convolutional network (ConvNet) to extract the shape feature from the foreground mask. The architecture of the MMDiT block in Flux-Pinco is illustrated in Fig. 9. Specifically, in addition to the conventional text-image MM-Attention block, Pinco introduces a text-image-condition MM-Attention mechanism. This design links the subject description in the text and image with the subject encoded in the condition, thereby enabling the model to correctly associate the subject in the text with the subject image provided by the condition, which helps to mitigate the issue of subject expansion. Furthermore, considering that both image and condition operations are performed at the image level, we employ HydraLoRA [57] to reduce the number of trainable parameters. HydraLoRA allows for efficient training by sharing the majority of parameters between the LoRA modules for the image and condition branches.

C. Derivation of SCPO

In Sec.3.4 in the main paper, we rewrite the Bradley-Terry (BT) model to learn the shared commonality preference between win-win pairs:

$$p_{\text{BT}}(\mathbf{x}_0^{w_1} \sim \mathbf{x}_0^{w_2} | c) = 1 - \sigma(|r(c, \mathbf{x}_0^{w_1}) - r(c, \mathbf{x}_0^{w_2})|). \quad (10)$$

RLHF aims to optimize a conditional distribution $p_\theta(x_0|c)$ (conditioning $c \sim \mathcal{D}_c$) such that the latent reward model

$r(c, x_0)$ defined on it is maximized, while regularizing the KL-divergence from a reference distribution p_{ref} :

$$\max_{p_\theta} \mathbb{E}_{c \sim \mathcal{D}_c, x_0 \sim p_\theta(x_0|c)} |r(c, x_0)| - \beta \mathbb{D}_{\text{KL}} [p_\theta(x_0|c) \| p_{\text{ref}}(x_0|c)]. \quad (11)$$

From [49], the unique global optimal solution p_θ^* becomes:

$$p_\theta^*(x_0|c) = p_{\text{ref}}(x_0|c) \exp(r(c, x_0)/\beta) / Z(c), \quad (12)$$

where $Z(c) = \sum_{x_0} p_{\text{ref}}(x_0|c) \exp(r(c, x_0)/\beta)$ is the partition function. Hence, the reward function is rewritten as:

$$r(c, x_0) = \beta \log \frac{p_\theta^*(x_0|c)}{p_{\text{ref}}(x_0|c)} + \beta \log Z(c). \quad (13)$$

To adapt SCPO to diffusion models, we introduce latents $x_{1:T}$ and define $R(c, x_{0:T})$ as the reward on the whole chain, such that we can define $r(c, x_0)$ as:

$$r(c, x_0) = \mathbb{E}_{p_\theta(x_{1:T}|x_0, c)} |R(c, x_{0:T})|. \quad (14)$$

As for the KL-regularization term in Eq. 11, following prior works [21, 54], we can instead minimize KL-regularization term's upper bound joint KL-divergence. So we have the objective:

$$\max_{p_\theta} \mathbb{E}_{c \sim \mathcal{D}_c, x_{0:T} \sim p_\theta(x_{0:T}|c)} |r(c, x_0)| - \beta \mathbb{D}_{\text{KL}} [p_\theta(x_{0:T}|c) \| p_{\text{ref}}(x_{0:T}|c)]. \quad (15)$$

With Eq. 10, the reward objective becomes:

$$L_{\text{SCPO}}(\theta) = -\mathbb{E}_{(x_0^{w_1}, x_0^{w_2}) \sim \mathcal{D}} \log \left(1 - \sigma \left(\beta \mathbb{E}_{\substack{x_{1:T}^{w_1} \sim p_\theta(x_{1:T}|x_0^{w_1}) \\ x_{1:T}^{w_2} \sim p_\theta(x_{1:T}|x_0^{w_2})}} \left| \log \frac{p_\theta(x_{0:T}^{w_1})}{p_{\text{ref}}(x_{0:T}^{w_1})} - \log \frac{p_\theta(x_{0:T}^{w_2})}{p_{\text{ref}}(x_{0:T}^{w_2})} \right| \right) \right). \quad (16)$$

Since sampling from $p_\theta(x_{1:T}|x_0^{w_1})$ is intractable, we utilize $q(x_{1:T}|x_0^{w_2})$ for approximation:

$$\begin{aligned} L_1(\theta) &= -\log \left(1 - \sigma \left(\beta \mathbb{E}_{\substack{x_{1:T}^{w_1} \sim q(x_{1:T}|x_0^{w_1}) \\ x_{1:T}^{w_2} \sim q(x_{1:T}|x_0^{w_2})}} \left| \log \frac{p_\theta(x_{0:T}^{w_1})}{p_{\text{ref}}(x_{0:T}^{w_1})} - \log \frac{p_\theta(x_{0:T}^{w_2})}{p_{\text{ref}}(x_{0:T}^{w_2})} \right| \right) \right) \\ &= -\log \left(1 - \sigma \left(\beta \mathbb{E}_{\substack{x_{1:T}^{w_1} \sim q(x_{1:T}|x_0^{w_1}) \\ x_{1:T}^{w_2} \sim q(x_{1:T}|x_0^{w_2})}} \left| \sum_{t=1}^T \log \frac{p_\theta(x_{t-1}^{w_1}|x_t^{w_1})}{p_{\text{ref}}(x_{t-1}^{w_1}|x_t^{w_1})} - \log \frac{p_\theta(x_{t-1}^{w_2}|x_t^{w_2})}{p_{\text{ref}}(x_{t-1}^{w_2}|x_t^{w_2})} \right| \right) \right). \end{aligned} \quad (17)$$

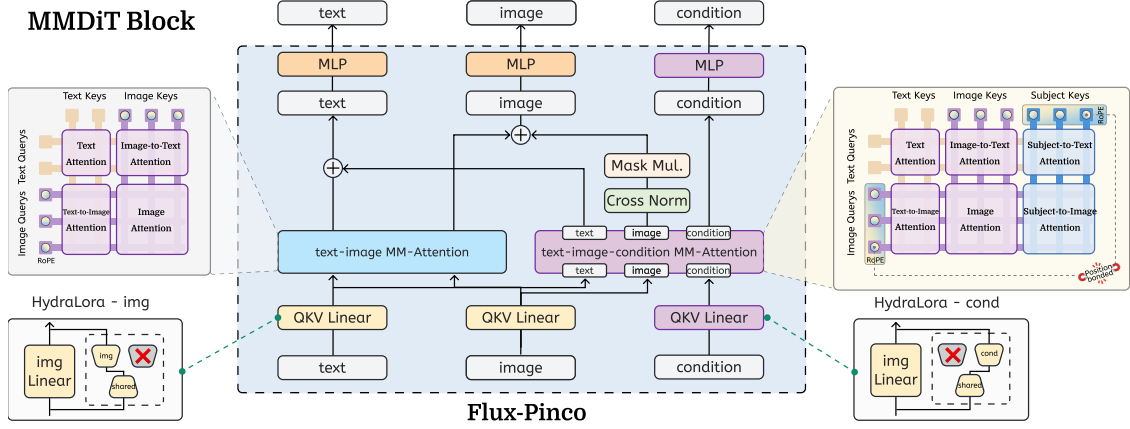


Figure 9. Architecture of Flux-Pinco, the base model of our InpaintDPO.

By Triangle inequality, we have:

$$\begin{aligned}
L_1(\theta) &\leq -\log \left(1 - \sigma \left(\beta \mathbb{E}_{\substack{x_{1:T}^{w_1} \sim q(x_{1:T}|x_0^{w_1}) \\ x_{1:T}^{w_2} \sim q(x_{1:T}|x_0^{w_2})}} \log \frac{p_\theta(x_{t-1}^{w_1}|x_t^{w_1})}{p_{\text{ref}}(x_{t-1}^{w_1}|x_t^{w_1})} - \log \frac{p_\theta(x_{t-1}^{w_2}|x_t^{w_2})}{p_{\text{ref}}(x_{t-1}^{w_2}|x_t^{w_2})} \right) \right) \\
&= -\log \left(1 - \sigma \left(\beta T \mathbb{E}_t \mathbb{E}_{\substack{x_{t-1,t}^{w_1} \sim q(x_{t-1,t}|x_0^{w_1}) \\ x_{t-1,t}^{w_2} \sim q(x_{t-1,t}|x_0^{w_2})}} \left| \log \frac{p_\theta(x_{t-1}^{w_1}|x_t^{w_1})}{p_{\text{ref}}(x_{t-1}^{w_1}|x_t^{w_1})} - \log \frac{p_\theta(x_{t-1}^{w_2}|x_t^{w_2})}{p_{\text{ref}}(x_{t-1}^{w_2}|x_t^{w_2})} \right| \right) \right). \tag{18}
\end{aligned}$$

With some algebra and applying Jensen's inequality, we have:

$$\begin{aligned}
L(\theta) &= -\mathbb{E}_{(x_0^{w_1}, x_0^{w_2}) \sim \mathcal{D}, t \sim \mathcal{U}(0, T)} \log \left(1 - \sigma \left(\beta T \left| \mathbb{D}_{\text{KL}}(q(x_{t-1}^{w_1}|x_0, x_t^{w_1}) \| p_\theta(x_{t-1}^{w_1}|x_t^{w_1})) \right. \right. \right. \\
&\quad - \mathbb{D}_{\text{KL}}(q(x_{t-1}^{w_1}|x_0, x_t^{w_1}) \| p_{\text{ref}}(x_{t-1}^{w_1}|x_t^{w_1})) \\
&\quad - \mathbb{D}_{\text{KL}}(q(x_{t-1}^{w_2}|x_0, x_t^{w_2}) \| p_\theta(x_{t-1}^{w_2}|x_t^{w_2})) \\
&\quad \left. \left. \left. + \mathbb{D}_{\text{KL}}(q(x_{t-1}^{w_2}|x_0, x_t^{w_2}) \| p_{\text{ref}}(x_{t-1}^{w_2}|x_t^{w_2})) \right| \right) \right). \tag{19}
\end{aligned}$$

Then, we can yield the final SCPO loss:

$$\begin{aligned}
L_{\text{SCPO}}(\theta) &= -\mathbb{E} \log \left(1 - \sigma \left(\beta T \omega(\lambda_t) \left(\|\epsilon^{w_1} - \epsilon_\theta(x_t^{w_1}, t)\|_2^2 - \|\epsilon^{w_1} - \epsilon_{\text{ref}}(x_t^{w_1}, t)\|_2^2 \right) \right. \right. \\
&\quad \left. \left. - \left(\|\epsilon^{w_2} - \epsilon_\theta(x_t^{w_2}, t)\|_2^2 - \|\epsilon^{w_2} - \epsilon_{\text{ref}}(x_t^{w_2}, t)\|_2^2 \right) \right) \right).
\end{aligned}$$

D. Evaluation Metrics

In this section, we provide a more detailed description of the evaluation metrics. We quantitatively evaluate the model's performance from the following four perspectives: Foreground Consistency, Spatial Rationality, Text-alignment, and Image Quality.

(1) **Foreground Consistency:** To evaluate the subject extension ratio, we employ the Object Extension Ratio (OER) [7] metric, which quantifies the spatial consistency between the foreground subject mask of the generated image and the corresponding ground truth subject mask. Specifically, we utilize BiRefNet [74] and SAM2.1 [50] respectively to segment the generated image, yielding an accurate foreground subject mask M . For foreground-conditioned inpainting where the subject's position is fixed, the subject mask of the original image, denoted as M_o , serves as the ground truth mask (where M_o is typically derived from the input mask m , i.e., $M_o = 1 - m$). The OER score is then computed as follows:

$$\text{OER} = \frac{\sum \text{ReLU}(M - M_o)}{\sum M_o}, \tag{20}$$

where $\text{ReLU}(\cdot)$ is the Rectified Linear Unit activation function. The OER metric quantifies the extension of the subject in the generated image relative to the ground truth. Therefore, a smaller OER score indicates superior subject consistency achieved by the inpainting model.

(2) **Spatial Rationality:** We leverage the GPT4o [1] to evaluate each image based on Spatial Scale, Positional Relationship, and Viewpoint. The assessing standard for these three aspects and rating criteria are as follows:

- **Spatial Scale:** Assess whether the size proportions between the subject and other objects in the image are realistic and whether there is any disproportion between the subject and surrounding objects.
- **Positional relationship:** Check whether the spatial rela-



Given Image



Subject

Task Description:
Analyze the physical relationship between the [subject] and the background in the given image. Utilize your visual abilities and understanding of the physical world to assess the realism of the image and provide a brief explanation.

Evaluation Guidelines:
Specifically, please evaluate the following aspects and score each item according to the rating criteria:
1. **Spatial Scale Relationship:** Assess whether the size proportions between the [subject] and other objects in the image are realistic, and whether there is any disproportion between the [subject] and surrounding objects.
2. **Positional Rationality:** Check whether the spatial relationship between the [subject] and other objects in the image is reasonable and consistent with common placement methods in daily life. Determine whether the [subject] is placed in a physically impossible position, such as floating.
3. **Viewpoint Rationality:** Verify if the perspective relationship between the [subject] and background is consistent with physical laws. The extension lines of the [subject] and its supporting surface should converge at a single background vanishing point, reflecting a normal perspective effect.

Rating Criteria:
- 1 point: Obvious errors, inconsistent with the real world.
- 3 points: Minor errors, somewhat inconsistent with the real world.
- 5 points: No obvious errors, consistent with the real world.

Please evaluate the Spatial Scale rationality, Positional rationality, and Viewpoint rationality in the image, provide three scores respectively, and briefly explain your reasoning. Think step by step to arrive at the final scores.

Reply:

- Object Placement Relationship: 5 points**
- The robotic vacuum and its dock are placed on the rug/floor, and the dog is positioned naturally near the cabinet. All objects are supported by surfaces (no floating), so this is consistent with the real world.
- Object Size Relationship: 5 points**
- The robotic vacuum, dock, dog, furniture, and decor all have proportions that match real-world sizes. For example, the dog is appropriately sized relative to the cabinet, and the vacuum is appropriately sized for a home appliance.
- Physical Space Relationship: 5 points**
- The perspective is consistent (objects appear as they would in a real living room), and the distances between objects (e.g., the vacuum and the dock, the dog and the cabinet) are reasonable. There are no distortions or unrealistic spatial gaps.

Overall, all aspects of object placement, size, and spatial distance align with real-world expectations, showing no errors.

Figure 10. GPT-4o prompt for assessment and its reply. Note that you need to specify the name of the subject in [subject].

relationship between the subject and other objects in the image is reasonable and consistent with common placement methods in daily life. Determine if the subject is placed in a physically impossible position, such as floating.

- **Viewpoint:** Examine whether the perspective extension direction of the product is consistent with that of its supporting surface. Judge if there is an unreasonable perspective relationship, such as mismatched horizontal lines or inconsistent convergence trends between the product and the supporting surface, which violates the basic principles of linear perspective.
- **Rating Criteria:** 1 point: Obvious errors, inconsistent with the real world. 3 points: Minor errors, somewhat inconsistent with the real world. 5 points: No obvious errors, consistent with the real world.

The detailed prompt given to GPT-4o and the reply are shown in Fig. 10. We also show some rationality analysis returned by GPT-4o under the criteria mentioned above, as shown in Fig. 16.

(3) **Text-alignment:** We evaluate text alignment from two aspects:

- To measure the text-image alignment, we follow Imagen3 [4] and adopt the Visual Question Answering (VQA) score [38]. This metric assesses the alignment between the generated image and the input text prompt by leverag-

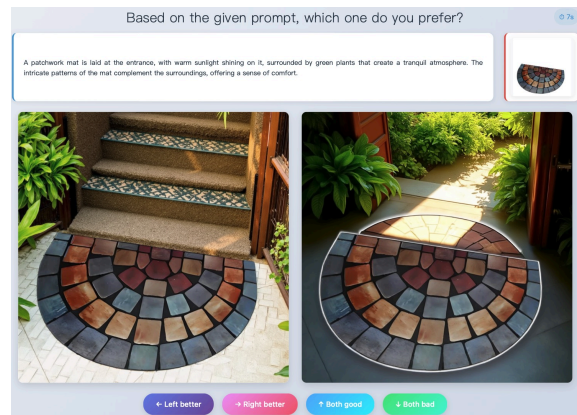


Figure 11. GUI of AI Inpainting Arena.

ing a VQA model to answer a series of simple yes-or-no questions regarding the image content.

- In the text-guided foreground-conditioned inpainting task, a common failure mode arises when the model redundantly generates the given foreground subject, often due to an inability to recognize the subject as already present based on the prompt. This often leads to generated results containing multiple similar subjects, which typically deviates from the user’s intent. To quantitatively

Table 6. Quantitative ablation studies on foreground-background coherence in CAPO.

Combination	Foreground Consistency OER(BIRefNet) ↓ OER(SAM2.1) ↓		Spatial Rationality Avg. ↑	Text-alignment VQA Score ↑	Image Quality FID ↓ Context ↑	
MaskDPO	5.6%	3.4%	3.93	0.863	98.87	0.250
MaskDPO-Expanded	5.8%	3.4%	3.87	0.862	99.31	0.252
MaskDPO+CAPO	5.6%	3.1%	3.93	0.866	97.42	0.258



Figure 12. Qualitative ablation study on CAPO.

to assess this failure, we utilize FlorenceV2 [62] to detect and count the number of the specified subject within the generated image given the subject’s name. Subsequently, the Multi-subject Rate is calculated as the ratio where the detected subject count exceeds the desired number of subjects. A higher Multi-subject Rate indicates poorer subject recognition and control.

(4) **Image Quality:** We evaluate the image quality from two aspects:

- To evaluate the perceptual quality of the generated images, we compute the Fréchet Inception Distance (FID) [20] score on the MSCOCO dataset [37].
- Following OmniPaint [69], we calculate the Context Coherence to quantify the structural consistency, since sometimes the foreground subject might exhibit structural misalignment with the surrounding background in the generated results. Specifically, denoting the foreground region as Ω_M and the background bounding box region excluding the foreground region as $\Omega_{B \setminus M}$, we compute the feature deviation by:

$$d_{\text{context}} = 1 - f(\Omega_M)^\top f(\Omega_{B \setminus M}), \quad (21)$$

where the feature embeddings $f(\Omega)$ are extracted using the pre-trained vision model DINOv2 [44].

E. User Study

To comprehensively evaluate the perceived quality and, crucially, the spatial rationality of the generated images, we conducted a large-scale human preference study using an AI Inpainting Arena platform. This setup employs the ELO rating system [15], a robust method traditionally used in competitive ranking, to accurately measure human preference for different inpainting methods. Specifically, users were presented with a pair of anonymously generated images, each produced by a different model but sharing the

identical input: the foreground image and the text prompt. The users’ task was to act as judges and select the better image between the two, as shown in Fig. 11. The primary criterion for the judgment was Spatial Rationality: the natural and visually consistent integration of the foreground subject within the generated background scene. This involves consideration of factors such as relative scale, spatial relationship, and viewpoint consistency between the foreground and the generated background.

We involved all the inpainting methods, including PowerPaint [75], BrushNet [28], SD3-ControlNet [14], OmniControl-inpaint [55], Flux-Fill-dev [33], Flux-ControlNet [13], Flux-Pinco [41], and our InpaintDPO under comparison in this arena. To ensure high-quality and reliable judgments, we invited over 30 experts specialized in computer vision and AIGC fields to participate. After the collection of over 10,000 votes across numerous model competitions, the final ELO scores are calculated and presented in Tab. 2 in main paper, where our InpaintDPO model ranks first with the highest ELO score. These results strongly validate that our method is significantly preferred by human, particularly regarding the crucial aspect of spatial rationality.

F. More Qualitative Comparisons

We provide more qualitative comparisons between our InpaintDPO with the state-of-the-art methods in Fig. 17, 18, and 19. The compared baselines include:

- Editing Methods: Flux-Kontext [34] and Qwen-Image-Edit [60];
- UNet-based Inpainting Methods: PowerPaint [75] and BrushNet [28];
- MMDiT-based Inpainting Methods: SD3-ControlNet [14], OmniControl-inpaint [55], Flux-Fill-dev [33], Flux-ControlNet [13] and Flux-Pinco [41].

Results show our InpaintDPO consistently achieves better background spatial relationship rationality, while also maintaining superior performance in foreground consistency and text alignment; while current SOTA methods suffer from spatial relationship hallucinations, e.g., incorrect layout arrangements and object interaction, or worse foreground subject preservation.

G. More Ablation Study

Boundary Artifacts Reduction. In the main paper, in Sec. 4.3, we introduce CAPO, which improves boundary coherence by guiding the model with a global preference loss. To verify the effectiveness of our method, we introduce another naive approach for comparison: applying the erosion operation to the background mask. This process is intended to expand the effective scope of the inpainting loss in the subject area, thus creating a transitional area out-

side of the foreground subject for two distinct optimization losses. The comparison results are shown in Fig. 12 and Tab. 6. Although the erosion can mitigate boundary artifacts, it ignores preference optimization in the transitional area, which includes foreground-background interaction information. Thus, it will to some extent affect the learning of positional rationality. Conversely, our CAPO not only maintains the integrity of MaskDPO and achieves superior boundary coherence, but also learns better positional rationality, thereby delivering superior performance in image quality and spatial rationality.

H. More Results of Method Migration

We apply our InpaintDPO to Qwen-Image-Edit to enhance its spatial rationality. Specifically, we finetuned the Qwen-Image-Edit model with LoRA based on the repo [43]. Since edit models often lack strong subject-following capability, we have increased the weight of the Inpainting Loss, where the hyperparameters λ, γ, μ are set to 5, 1, and 0.5, respectively. More results are shown in Fig. 20. Results show applying our InpaintDPO successfully enabled the image editing model to achieve better subject detail preservation and improved spatial rationality, validating our InpaintDPO’s generalizability.

I. More Results of Different Aspect Ratios

We show more generation results with different aspect ratios. As illustrated in Fig. 13, 14 and 15, our InpaintDPO generates high-quality inpainting results, with superior performance especially in background spatial rationality.

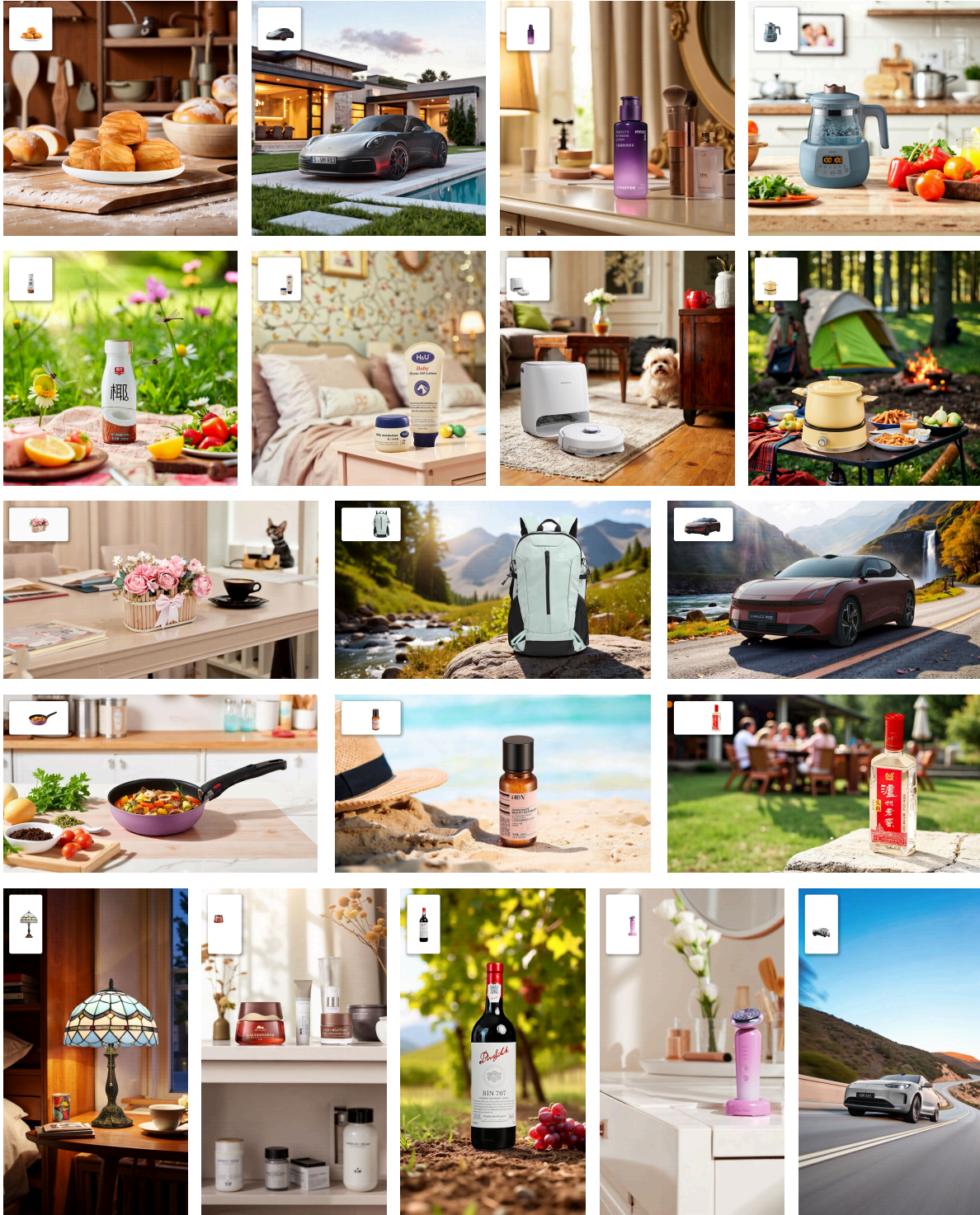


Figure 13. More cases generated by InpaintDPO. InpaintDPO supports the generation of high-quality images with different aspect ratios, while ensuring the reasonable placement of subjects, achieving realistic foregroundconditioned inpainting.

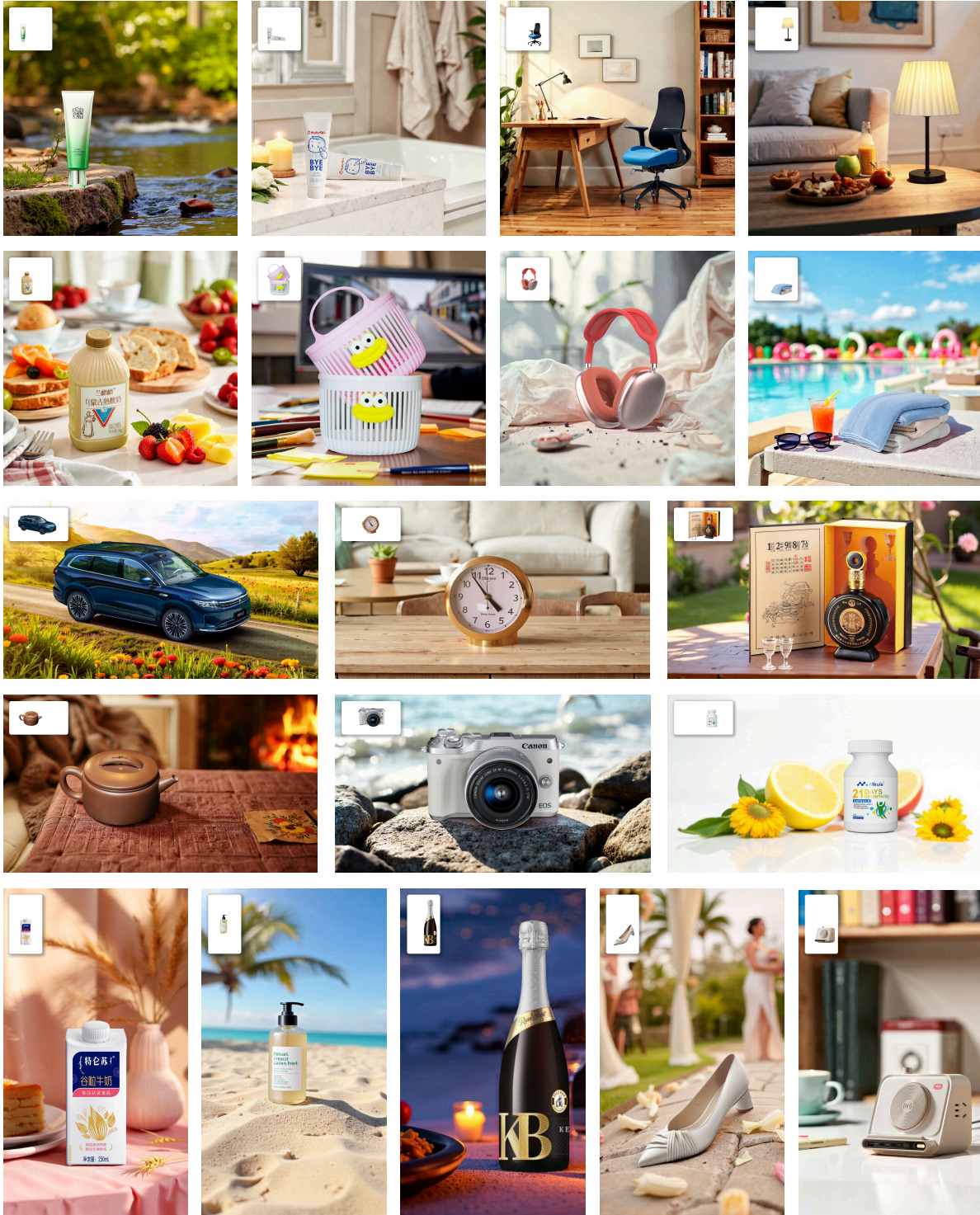


Figure 14. More cases generated by InpaintDPO. InpaintDPO supports the generation of high-quality images with different aspect ratios, while ensuring the reasonable placement of subjects, achieving realistic foregroundconditioned inpainting.

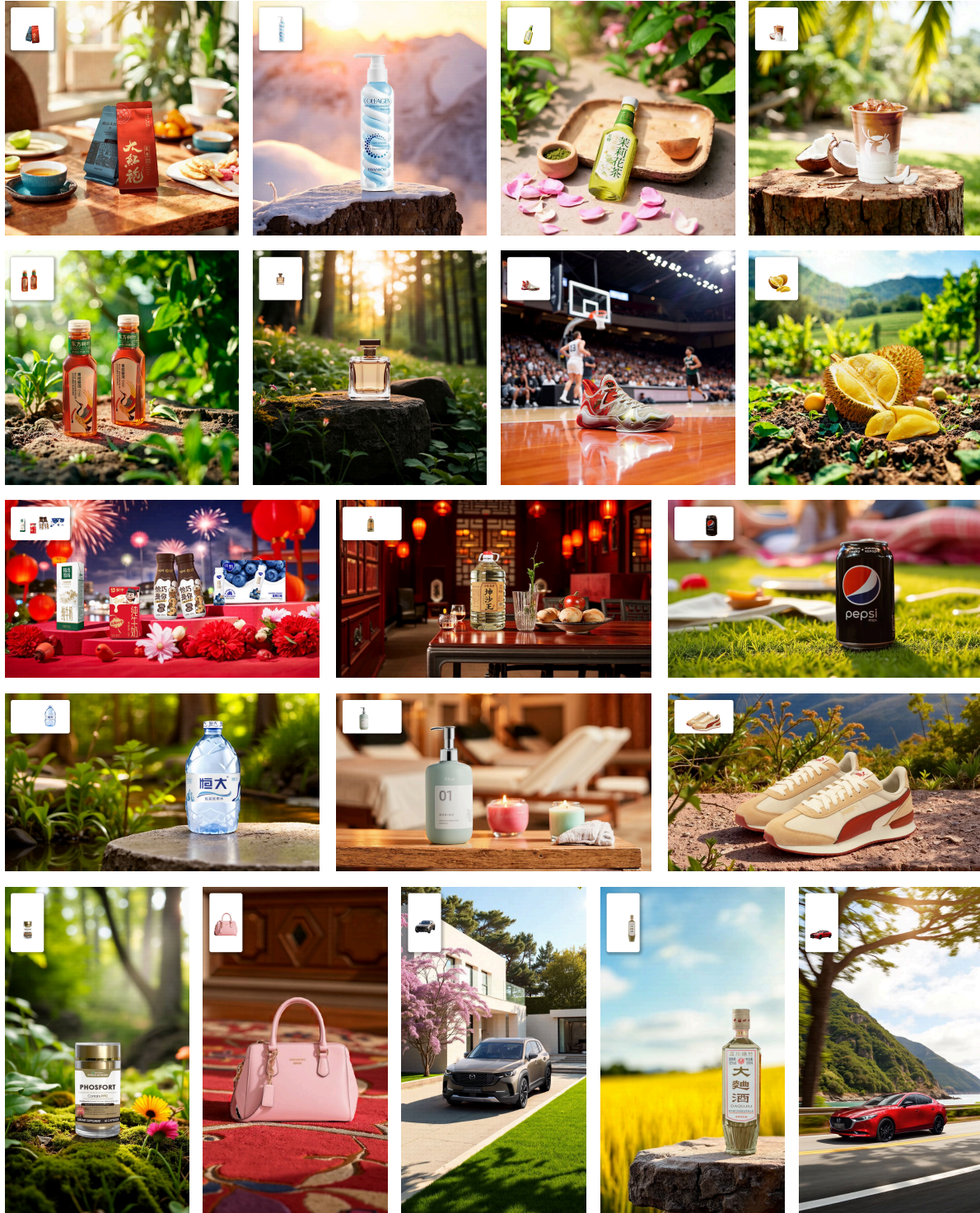


Figure 15. More cases generated by InpaintDPO. InpaintDPO supports the generation of high-quality images with different aspect ratios, while ensuring the reasonable placement of subjects, achieving realistic foregroundconditioned inpainting.

Spatial Scale Rationality



Subject



Score: 1.0

The spatial scale of the semiconductor laser therapeutic device, its packaging box, and the background exhibition hall is severely inconsistent.



Score: 3.0

The semiconductor laser therapeutic device is slightly larger than typical smartwatch-sized medical wearables. The minor size deviation aligns with common product exhibition enlargement needs.



Score: 5.0

The semiconductor laser therapeutic device, the packaging box, and the small accessories around them form a clear and reasonable hierarchical structure.

Positional Rationality



Subject



Score: 1.0

The jade bangle is floating in mid-air without any physical support, which is inconsistent with the real world's gravity and physical laws.



Score: 3.0

The jade bangle is placed on the sandy surface, which is physically reasonable. The shadow and the interaction between the bangle and the sand have minor inconsistencies in detail.



Score: 5.0

The jade bangle is placed on the wooden plank, with a stable position and a shadow that conforms to the light source.

Viewpoint Rationality



Subject



Score: 1.0

The car is floating in the air. The perspective lines of the car and the background elements do not converge at a single vanishing point, resulting in a completely inconsistent and physically implausible viewpoint.



Score: 3.0

The perspective relationship between the car, sheep, and the road is mostly consistent, with minor discrepancies in the convergence of perspective lines, especially in the proportion and spatial integration of the road.



Score: 5.0

The perspective lines of the car, road, and surrounding trees converge at a single vanishing point, and the spatial relationship is completely consistent with real-world perspective laws, without any obvious errors.

Figure 16. GPT4o rationality analysis results

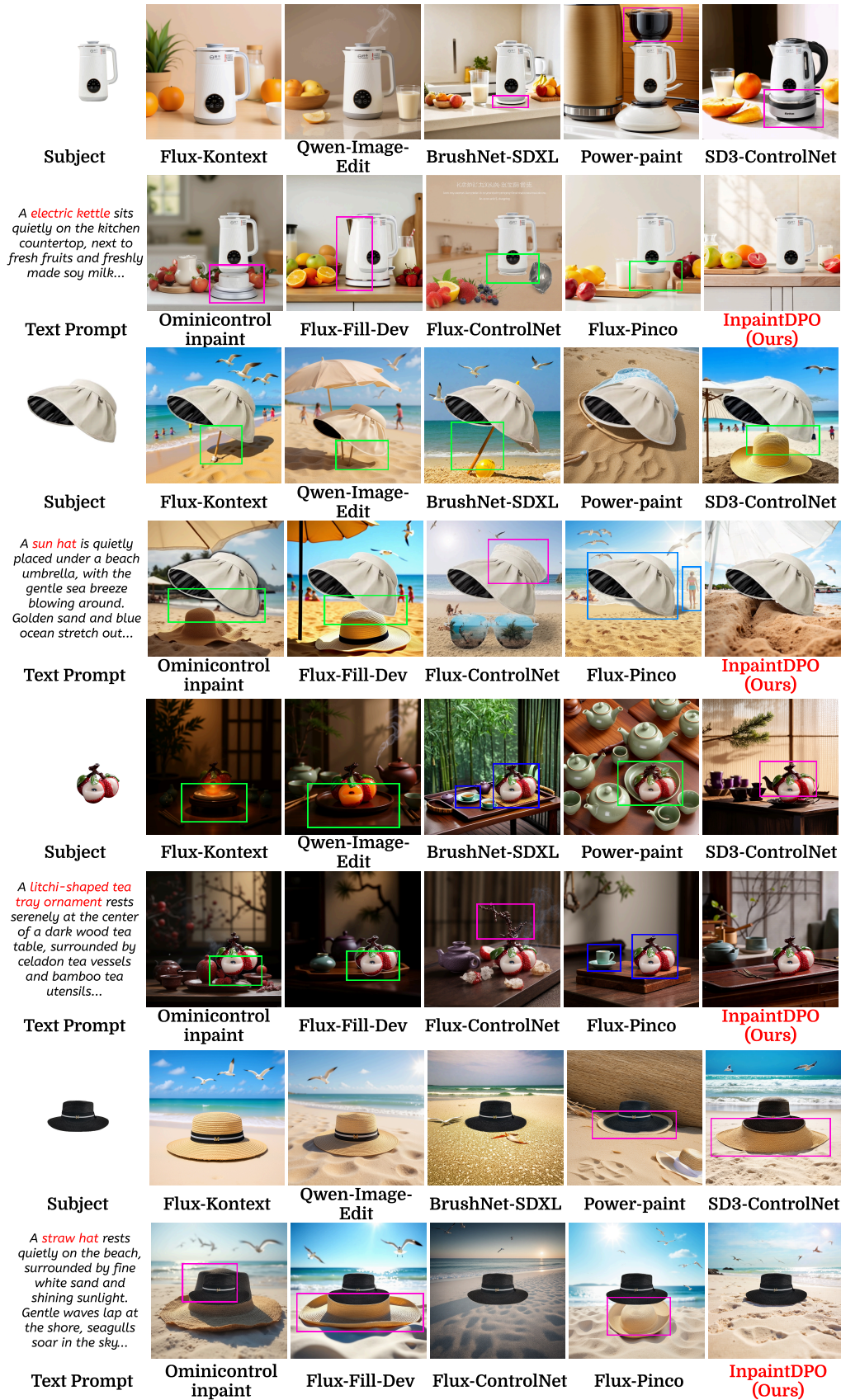


Figure 17. More qualitative comparisons between our InpaintDPO and the state-of-the-art methods. We highlight the unreasonable extension parts with pink boxes, inappropriate positional relationship with green boxes and inappropriate viewpoint with orange boxes, and label the inappropriate spatial scale with blue. Please zoom in for more details.

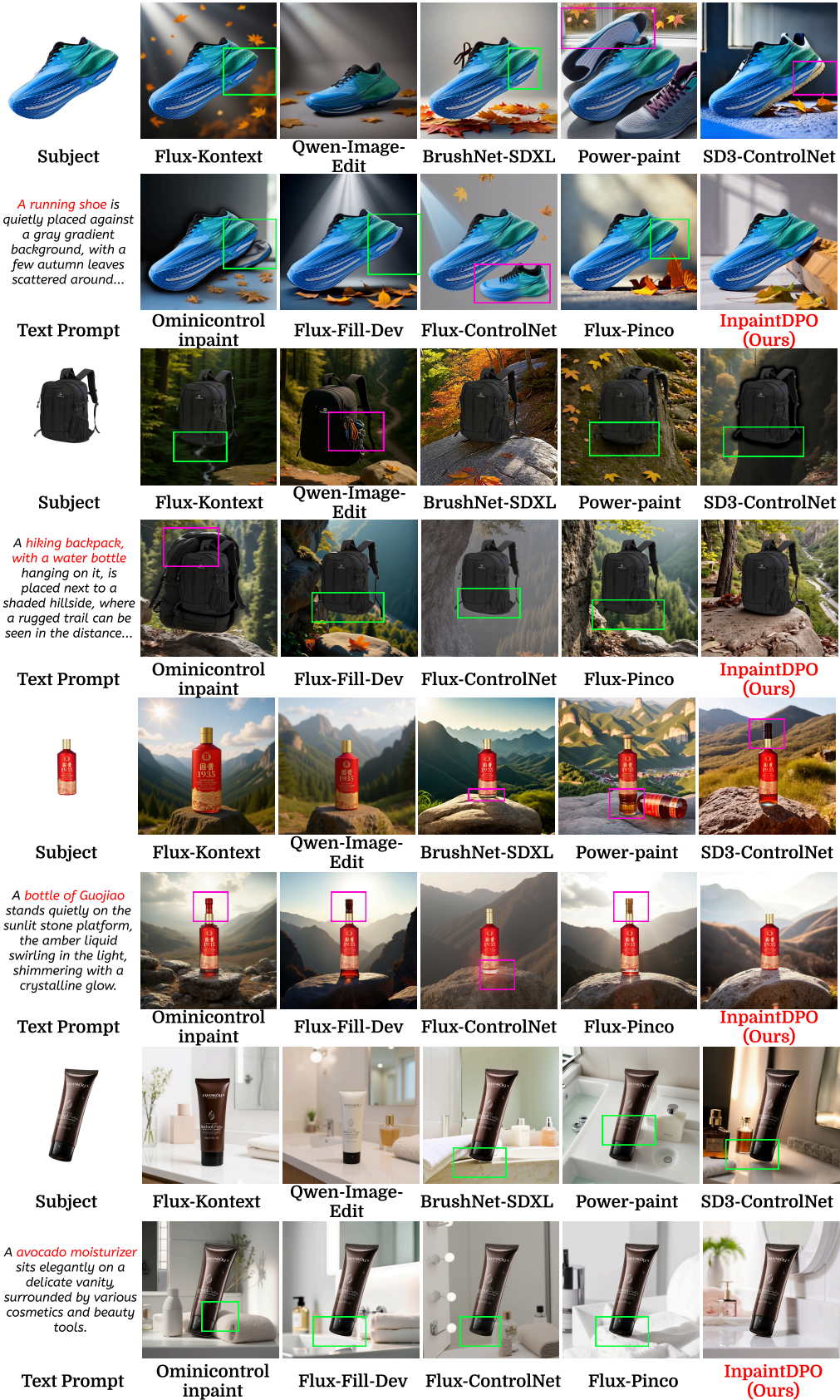


Figure 18. More qualitative comparisons between our InpaintDPO and the state-of-the-art methods. We highlight the unreasonable extension parts with pink boxes, inappropriate positional relationship with green boxes and inappropriate viewpoint with orange boxes, and label the inappropriate spatial scale with blue. Please zoom in for more details.



Figure 19. More qualitative comparisons between our InpaintDPO and the state-of-the-art methods. We highlight the unreasonable extension parts with pink boxes, inappropriate positional relationship with green boxes and inappropriate viewpoint with orange boxes, and label the inappropriate spatial scale with blue. Please zoom in for more details.

A **stainless steel cart** is placed in a spacious and bright kitchen. A modern rice cooker and several spice jars sit on the countertop...



A **Guizhou Prince Wine** is neatly placed on the supermarket shelf, surrounded by a dazzling array of products and passing customers...



A **lighter** rests on a simple rectangular panel, surrounded by soft lighting and bright colors that create a youthful and pleasant atmosphere...



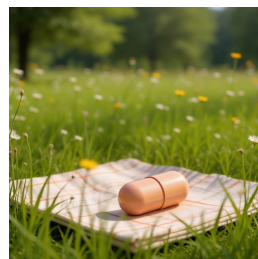
A **electric shaver** is placed beside a travel bag, next to a neatly packed suitcase and various travel essentials, ready to embark on a new journey...



A **Estee Lauder Advanced Night Repair** sits elegantly on the bathroom counter, illuminated by bright lights that enhance the clean and tidy atmosphere.



A **Orlistat capsule** is placed on a sunny picnic cloth in the wild, surrounded by lush green grass and blooming wildflowers...



Text Prompt

Subject

Qwen-Image-Edit

Qwen-InpaintDPO

Figure 20. More comparison between Qwen-Image-Edit and Qwen-InpaintDPO